

***AB INITIO* CALCULATIONS OF ELECTRONIC, ELASTIC AND  
SUPERCONDUCTIVITY PROPERTIES OF HEXAGONAL  
ANTIPEROVSKITE- TYPE CARBIDES  $XCr_3$  (X=Al, Ga or Zn) MATERIALS**

**DAVID N. MAINA**


**A Thesis Submitted to the Institute of Postgraduate Studies of Kabarak University  
in Partial Fulfillment of the Requirements for the Award of the Master of Science  
in Physics**

**KABARAK UNIVERSITY**

**NOVEMBER, 2024**

## DECLARATION

1. I do by declare that:
  - i. This thesis is my work and to the best of my knowledge, it has not been presented for the award of a degree in any university or college.
  - ii. That the work has not incorporated material from other works or a paraphrase of such material without due and appropriate acknowledgment.
  - iii. That the work has been subjected to processes of anti-plagiarism and has met Kabarak University 15% similarity index threshold.
2. I do understand that issues of academic integrity are paramount and therefore I may be suspended or expelled from the University or my degree may be recalled for academic dishonesty or any other related academic malpractices.

Signature: 

Date: 8/11/2024

David N. Maina

GMP/M/0345/01/20

## RECOMMENDATION

To the Institute of Postgraduate Studies:

The research project entitled “*Ab Initio* Calculations of Electronic, Elastic and Superconductivity Properties of Hexagonal Antiperovskite- Type Carbides  $XCr_3$  ( $X=Al, Ga$  Or  $Zn$ ) Materials” written by **David N. Maina** is presented to the Institute of Postgraduate Studies of Kabarak University. We have reviewed the research project and recommend it be accepted in partial fulfillment of the requirement for the award of the degree of Master of Science in Physics.


Signature: 

Date: 8/11/2024

Dr. Philip Otieno Nyawere

Department of Physical and Biological Sciences

Kabarak University.

Signature: 

Date: 6/11/2024

Dr. Elica Wabululu

Department of physics

Catholic University of Eastern Africa.

## **COPYRIGHT**

© 2024

David N. Maina

All rights reserved. No part of this Thesis may be reproduced or transmitted in any form using either mechanical, including photocopying, recording, or any other information storage or retrieval system without permission in writing from the author or Kabarak University.

## **ACKNOWLEDGEMENT**

First, I thank Almighty God for his sufficient grace and mercies which are new each morning without which the completion of this study will not have been possible. I appreciate my supervisors Dr. Philip Otieno Nyawere and Dr. Elicah Wabululu for their expertise, dedication, drive, encouragement and necessary support needed to make this project a success.

My gratitude goes to my family; parents Mr. Johnson Njuguna and Mrs Gladys Muthoni, my brother Samwel Wainaina and my dear wife Loise Kiragu for their prayers, financial support and moral support.

I am very grateful to the Centre for High Performance Computing (CHPC), South Africa for providing the computational resources which led to the success of this study I also thank Kabarak University from the bottom of my heart for the incredible opportunity they gave me.

## **DEDICATION**

I dedicate the work of this study to my beloved wife Loise, my daughter Gladys, my parents and siblings for their unwavering support during the study.

## ABSTRACT

The positions of the anions and cations are switched in antiperovskites material, which are inorganic compounds with a perovskite-like structure. The family of antiperovskites materials includes insulators, superconductors and semiconductors which make them useful in a variety of technologies such as spintronics, memory devices, transformers, motors, generators and sensors. There has not been enough research done on how magnetism and superconductivity interact. Antiperovskite hexagons' superconducting transition temperatures have not been fully studied. To complement experiments, computational simulations must be developed. The analysis of the superconducting properties in detail, including the superconducting energy gap, electronic structure properties and superconducting transition temperature, was done using a state-of-the-art *ab initio* approach. The Quantum Espresso Simulation Package was used to run all the calculations. Density functional theory as well as plane wave basis set framework were used for all computations. The electronic structure properties, elastic, superconducting transition temperatures and thermodynamic properties of hexagonal antiperovskite  $XCCr_3$  ( $A=Zn, Ga, \text{ or } Al$ ) were all calculated using density functional theory in the generalized gradient approximation (GGA). The calculated lattice constants were  $5.207\text{\AA}$ ,  $5.813\text{\AA}$  and  $5.721\text{\AA}$  for  $AlCCr_3$ ,  $GaCCr_3$  and  $ZnCCr_3$  respectively and are in good agreement with the previous available theoretical work. Voigt-Reuss-Hill averaging was used to obtain values for the parameters that make up the elastic constants. From this study,  $AlCCr_3$ ,  $GaCCr_3$  and  $ZnCCr_3$  were all found to have Poisson's ratios of 0.1114, 0.1153 and 0.094 respectively. Each parameter calculated value was checked against previously established theoretical and experimental norms. The transition temperature of the three materials is investigated so that the electron-phonon interaction may be simulated. Phonon dispersion research confirmed that all three compounds are dynamically stable. The mechanism for superconductivity is the interaction of electrons in the 4d state of Cr with low-frequency phonons. The average electron-phonon coupling value was calculated to be 0.60 for  $AlCCr_3$ , 0.77 for  $GaCCr_3$ , and 0.70 for  $ZnNCCr_3$ , yielding superconducting transition temperatures of 6.82 K, 12.01 K and 8.21 K, respectively indicating a moderate amount of electron-phonon coupling strength. The findings show that compared to  $GaCCr_3$  and  $ZnCCr_3$ ,  $AlCCr_3$  is harder, stiffer, and more tightly bound, and has a Debye temperature that is much higher. However, at lower Debye temperatures, the bonds in  $GaCCr_3$  and  $ZnCCr_3$  are weaker and the materials are less stiff.

**KeyWords:** *Antiperovskite, Density Functional Theory, First Principle, Superconductivity*

## TABLE OF CONTENTS

<b>DECLARATION</b> .....	<b>ii</b>
<b>RECOMMENDATION</b> .....	<b>iii</b>
<b>COPYRIGHT</b> .....	<b>iv</b>
<b>ACKNOWLEDGEMENT</b> .....	<b>v</b>
<b>DEDICATION</b> .....	<b>vi</b>
<b>ABSTRACT</b> .....	<b>vii</b>
<b>TABLE OF CONTENTS</b> .....	<b>viii</b>
<b>LIST OF TABLES</b> .....	<b>xi</b>
<b>LIST OF FIGURES</b> .....	<b>xii</b>
<b>ABBREVIATIONS AND ACRONYMS</b> .....	<b>xiii</b>
<b>OPERATIONAL DEFINITION OF KEY TERMS</b> .....	<b>xv</b>
<b>CHAPTER ONE</b> .....	<b>1</b>
<b>INTRODUCTION</b> .....	<b>1</b>
1.1 Overview .....	1
1.2 Background of the Study.....	1
1.3 Statement of the Research Problem .....	3
1.4 Objectives of the Study .....	3
1.4.1 General Objective of the Study .....	3
1.4.2 Specific Objectives of the Study .....	4
1.5 Research Questions .....	4
1.6 Justification of the Study.....	4
1.7 Significance of the Study .....	5
1.8 Scope of the Study .....	5
1.9 Assumptions.....	5
<b>CHAPTER TWO</b> .....	<b>6</b>
<b>LITERATURE REVIEW</b> .....	<b>6</b>
2.1 Introduction.....	6
2.2 Electronic Structure Properties of Hexagonal Antiperovskite Material .....	6
2.3 Elastic Properties of Hexagonal Antiperovskite .....	8
2.4 Superconductivity Properties .....	10
2.5 Thermodynamic Properties .....	11
2.6 Research Gaps.....	12



2.7 Conceptual Framework .....	13
<b>CHAPTER THREE.....</b>	<b>14</b>
<b>RESEARCH DESIGN AND METHODOLOGY .....</b>	<b>14</b>
3.1 Introduction .....	14
3.2 Description of the Working of Quantum Espresso .....	14
3.3 Electronic Structure Properties .....	16
3.4 Elastic Properties.....	17
3.5 Superconductivity Properties .....	20
3.6 Thermodynamic Properties .....	22
3.7 Derivation of the Governing Equations and Theorems .....	24
3.7.1 The Many Body Problem .....	24
3.7.2 Electronic Density .....	27
3.7.3 Hartree-Fock Approximation .....	29
3.8 Density Functional Theory.....	30
3.8.1 Hohenberg and Kohn Theorem .....	32
3.8.2 The Kohn-Sham equation.....	34
3.8.3 Exchange-Correlation Approximation .....	35
3.8.4 Local Density Approximation (LDA) .....	35
3.8.5 Generalized Gradient Approximation (GGA).....	36
3.8.6 Hybrid Functional.....	37
3.8.7 The Perdew, Burke, Ernzerhof Exchange Correlation Functional .....	37
3.9 Plane Waves .....	38
3.10 Energy Cut-off .....	40
3.11 K-Points .....	41
3.12 Pseudopotential Approximation.....	42
3.12.1 Norm conserving pseudopotential.....	43
3.12.2 Ultra Soft Pseudo-Potential .....	43
3.13 Self-consistent Field (scf) Cycle .....	45
<b>CHAPTER FOUR .....</b>	<b>49</b>
<b>RESULTS AND DISCUSSION .....</b>	<b>49</b>
4.1 Introduction .....	49
4.2 Electronic Structural Properties of Hexagonal Antiperovskite.....	49
4.2.1 Structural Properties .....	49

4.2.2 Electronic Properties .....	50
4.2.3 Density of States.....	51
4.3 Elastic properties.....	52
4.3.1 Elastic Anisotropy .....	52
4.3.2 Debye Temperature .....	55
4.4 Superconductivity Properties .....	56
4.5 Thermodynamic Properties .....	60
<b>CHAPTER FIVE .....</b>	<b>64</b>
<b>SUMMARY, CONCLUSION AND RECOMMENDATIONS .....</b>	<b>64</b>
5.1 Introduction.....	64
5.2 Summary .....	64
5.2.1 Electronic Structure Properties.....	64
5.2.2 Elastic Properties .....	64
5.2.3 Superconductivity Properties .....	65
5.2.4 Thermodynamic Properties .....	65
5.3 Conclusion .....	65
5.4 Recommendations for Further Research.....	66
<b>REFERENCES .....</b>	<b>67</b>
<b>APPENDICES.....</b>	<b>74</b>
<b>Appendix I: Input File for Pwscf Code AlCCr3 Structure .....</b>	<b>74</b>
<b>Appendix II: Input File for Pwscf Code GaCCr3 Structure.....</b>	<b>76</b>
<b>Appendix III: Input File for Pwscf Code ZnCCr3 Structure .....</b>	<b>78</b>
<b>Appendix IV: Output File for AlCCr3 Structure.....</b>	<b>80</b>
<b>Appendix V: Output File for GaCCr3 Structure .....</b>	<b>84</b>
<b>Appendix VI: Output File for ZnCCr3 Structure .....</b>	<b>88</b>
<b>Appendix VII: Introduction letter from the institution .....</b>	<b>92</b>
<b>Appendix VIII: KUREC Clearance Letter.....</b>	<b>93</b>
<b>Appendix IX: NACOSTI Research Permit .....</b>	<b>94</b>
<b>Appendix X: Evidence of Conference Participation .....</b>	<b>95</b>
<b>Appendix XI: List of Publications.....</b>	<b>96</b>

## LIST OF TABLES

<b>Table 1:</b> Calculated lattice constants in ( $\text{\AA}$ ) and elastic constants in GPa.....	52
<b>Table 2:</b> Shear type anisotropic ratios compared to results from other Studies .....	53
<b>Table 3 :</b> A comparative analysis of the results related to Young Modulus, E in Gpa, Poisson ratio $\sigma$ , and Pugh Ratio (GH/BH), alongside the Bulk Modulus and Shear Modulus in Gpa, employing the Voigt, Reuss, and Hill Averaging Scheme.....	55
<b>Table 4 :</b> A comparison between the values obtained by the use of the Voigt-Reuss-Hill Average method for Compressional ( $V_P$ ), Bulk ( $V_B$ ), Shear ( $V_G$ ), Average Debye Sound Velocities ( $V_D$ ), Solid Density $\rho(g/cm^3)$ , and Debye Temperature $\Theta_D$ (K), and the corresponding values reported in earlier studies. ....	56
<b>Table 5 :</b> Density of States (DOS) near the Fermi level and the average electron-phonon coupling parameter ( $\lambda$ ), the logarithmic frequency ( $\omega_{ln}$ ), and the superconducting transition temperature for the hexagonal $XCCr_3$ (A=Al, Ga, or Zn) for this research, as well as a comparison with the results of available previous studies. ....	57

## LIST OF FIGURES

<b>Figure 1:</b> Unit Cell of Hexagonal Antiperovskite .....	8
<b>Figure 2:</b> Conceptual Framework .....	13
<b>Figure 3:</b> Total Energy Convergences with Plane Wave Cut-Off .....	40
<b>Figure 4:</b> Energy vs. K-Points Graph .....	42
<b>Figure 5:</b> Computational schematic representation of the S-C loop for the solution of the K-S Equation .....	47
<b>Figure 6:</b> Crystal Structure of Unit Cell of AlCCr <sub>3</sub> .....	49
<b>Figure 7:</b> Band structures of (a) AlCCr <sub>3</sub> , (b) GaCCr <sub>3</sub> and (c) ZnCCr <sub>3</sub> .....	50
<b>Figure 8:</b> Densities of the states of (a) AlCCr <sub>3</sub> , (b) GaCCr <sub>3</sub> and (c) ZnCCr <sub>3</sub> .....	51
<b>Figure 9</b> :Phonon frequency curves for (a) AlCCr <sub>3</sub> , (b) GaCCr <sub>3</sub> and (c) ZnCCr <sub>3</sub> along the hexagonal Brillouin zone symmetry lines.....	59
<b>Figure 10:</b> A plot of phonon densities of states of (a) AlCCr <sub>3</sub> , (b) GaCCr <sub>3</sub> and (c) ZnCCr <sub>3</sub> .....	60
<b>Figure 11:</b> Debye energy of vibration (KJ/Nmol) of (a) AlCCr <sub>3</sub> , (b) GaCCr <sub>3</sub> and (c) ZnCCr <sub>3</sub> over different temperatures. ....	61
<b>Figure 12:</b> Debye heat capacity C <sub>V</sub> (J/K/(Nmol)) of (a) AlCCr <sub>3</sub> , (b) GaCCr <sub>3</sub> and (c) ZnCCr <sub>3</sub> at various temperatures.....	62
<b>Figure 13:</b> Debye vibrational free energy (J/K/(Nmol)) of (a) AlCCr <sub>3</sub> , (b) GaCCr <sub>3</sub> and (c) ZnCCr <sub>3</sub> at various temperatures. ....	63

## ABBREVIATIONS AND ACRONYMS

A	Atomic mass
Al	Aluminium
APW	Augmented Plane Waves
BCS	Bardeen-Cooper-Schrieffer
BOA	Born-Oppenheimer Approximation
CASTEP	Cambridge Serial Total Energy Package
CHPC	Center for High Performance Computing
C	Carbon
Cr	Chromium
DFT	Density Functional Theory
DFPT	Density Functional Perturbation Theory
ESPRESSO	opEn-Source Package for Research in Electronic Structure, Simulation and Optimization
EPC	Electron Phonon Coupling
$E_{xc}$	The kinetic energy of a system's exchanges and correlations
$E_{cut}$	Plane wave cutoff energy
$E_v$	Electron volt unit
$E_{gap}$	Band gap energy
EV-GGA	Engel Vosko Generalized Gradient Approximation
FP	Full Potential
$F[n(r)]$	Functional of density
FORTRAN	Formula Translation
GGA	Generalized Gradient Approximation
GMR	Giant Magneto Resistance
Gpa	Gigapascals
GRACE	Graphing Advanced Computing and Exploration of data
G	Reciprocal lattice vectors
Ga	Galium
H	Hamiltonian operator
$i, j$	Band index
K	Kelvin
LO	Local Orbital

MATLAB	Matrix Laboratory
Me	Electron mass
MBJ	Modified Becke-Johnson
MP	Monkhorst Pack
MRI	Magnetic Resonance Imaging
MEMS	Micro Electro Mechanical Systems
$n(r)$	Electron charge density
$n \downarrow$	The density of electrons in their spin-down configuration
$n \uparrow$	Density of electrons in spin-up
PAW	Projected Augmented Wave
PBE	Perdew-Burke-Ernzerhof
PW	Plane Wave
Pwscf	Plane-Wave-Self-Consistent Field
QE	Quantum Espresso
$r$	A Crystal Point
$r'$	A reciprocal lattice point
Scf	self-consistent field
TE	Thermoelectric
Te	Kinetic energy of electrons
$T_C$	Transition temperature
USPP	Ultra-soft pseudopotential
$V_{\text{ion-e}}$	Electron-ion potential energy
$V_{\text{ext}}$	External potential
$V_H$	Hartree potential
$V^{\text{ps}}$	Pseudo-potential
XcrysDen	X-window Crystalline Structure and density
Z	Number of protons
Zn	Zinc
$\psi$	Many electron wave function
$\phi$	Coulomb potential
$\nabla$	Gradient operator/ Laplacian operator
$\Omega$	Cell volume

## OPERATIONAL DEFINITION OF KEY TERMS

**Electronic Properties** these are parameters and representations that describe the state and the behavior of electrons in a material.

**Young's Modulus** is the tensile stress in a material divided by the applied force per unit area.

**Bulk Modulus** is the ratio of the change in volume due to a uniformly applied compressive or tensile stress across the whole surface area of a substance.

**Shear Modulus (G)** it is a measurement of a material's elastic shear stiffness and is identified by the relationship between shear stress and shear strain.

**Anisotropy Factor (E)** it represents the probability density for a single scattering direction.

## CHAPTER ONE

### INTRODUCTION

#### 1.1 Overview

The background of the theories behind antiperovskite materials' superconductivity is addressed in this section. It then goes on to establish the significance and scope of the study, state the research topic, objectives and list of research questions.

#### 1.2 Background of the Study

The positions of the anions and cations are switched in antiperovskite materials, which are inorganic compounds with a perovskite-like structure (Krivovichev, 2008). A stream of electron pairs flowing without resistance in specific materials at low temperatures is a phenomenon that is explained by the BCS theory. Due to their wide variety of band gaps, antiperovskite materials are extremely useful and employed in various industrial applications (Okoye, 2006) where waste heat is immediately transformed to electrical energy in thermoelectric systems.

Giant Magneto Resistance, almost zero temperature coefficients of resistivity (Sun et al., 2010) and magnetostriction (Takenaka & Takagi, 2005) are just a few of the materials' intriguing physical properties. Due to its unique properties, antiperovskite is widely used to make devices like magnetic field sensors used for data retrieval, micro-electron mechanical systems, biosensors as well as hard drives (Asano *et al.*, 2008). Since their coefficient of resistance is zero across all temperatures, they are useful in every setting. Excellent mechanical properties of antiperovskites make them potentially useful in automotive and space technologies (Tong & Sun, 2012). They are strong mechanically and light in weight (Tong & Sun, 2012).



Due to the constantly expanding population, modern civilization has an increasing need for energy. There is always a need for reliable electrically conducting materials. The necessity to address the energy crisis served as a major motivator for interest in the research of these antiperovskite materials. Due to their excellent thermoelectric properties, antiperovskites have a significant potential to address the energy problem (Ovsyannikov & Shchennikov, 2010).

The electronic Schrödinger equation may be solved using first principle computation, a quantum mechanical technique, by knowing the locations of the system's nuclei and the amount of electrons. In order to examine the majority of attributes, including structural, electronic, mechanical and physical properties, a numerical simulation approach is required.

Researchers may use band structure simulations as a powerful theoretical tool for predicting these properties. Theorists now have a new tool at their disposal, made possible by the advent of modern, high-powered computers. Modern computers can do a broad variety of mathematical operations, including the solution of exceedingly complex equations and the manipulation of theories that can be extremely tough for mathematician. Therefore, with the advent of contemporary, high-performance computers and electronic structure computations have been more useful in the physics and chemistry fields during recent years. When beginning with an atomic model, modern approaches may describe the electronic properties and ground state structure of a system in great detail. In the first part of the twenty-first century, quantum theory was formulated and developed, resulting in much interest and understanding of basic concepts of physics. The relevance of quantum mechanics in both the pure and practical sciences is generally agreed upon, and its astounding degree of accuracy and predictability has been shown. It is self-evident that the fundamental equations that can

be solved are those of quantum mechanics when one is to find a description of genuine processes and actual materials. In order to make any meaningful progress, numerical solutions to the equations are required.

Density functional theory (DFT), a theory that correlates multi body systems used in computational physics or chemistry, is employed for the first principle analysis of electronic structure and magnetic properties of materials in their ground state under pressure or with temperature modification. In order to describe the quantum behavior of atoms and molecules, DFT is used to solve the Schrödinger equation, which takes into account real-world constraints. First principles calculations based on DFT were performed to determine the superconductivity properties, structural, electronic, and elastic properties of  $XCCr_3$  ( $A=Zn, Ga, \text{ or } Al$ ).

### 1.3 Statement of the Research Problem

The mechanisms for superconductivity of antiperovskite have not been fully understood. The influence of phonon dispersion on the electron-phonon coupling constant has not explicitly been stated. This research focused on *ab initio* study of the superconductivity properties of hexagonal antiperovskite  $XCCr_3$  ( $X=Zn, Ga \text{ or } Al$ ). Computational calculations were employed where simulation of the properties of material under study were carried out.

## 1.4 Objectives of the Study

### 1.4.1 General Objective of the Study

This research sought to use the *ab initio* approach to determine the elastic, electronic structure, superconducting, and thermodynamic properties of  $XCCr_3$  ( $X=Zn, Ga, \text{ or } Al$ ).

### **1.4.2 Specific Objectives of the Study**

The objectives of this study were:

- i. To use first principles methodology to determine the electronic structure properties of hexagonal antiperovskite materials  $XCCr_3$  ( $X=Zn, Ga$  or  $Al$ ).
- ii. To use the first principles technique to determine the elastic properties of  $XCCr_3$  ( $X=Zn, Ga, or Al$ ).
- iii. To use the first principles technique to determine the superconducting properties of the hexagonal antiperovskite materials  $XCCr_3$  ( $X=Zn, Ga, or Al$ ).
- iv. To use density functional theory technique to determine the thermodynamic properties of the materials  $XCCr_3$  ( $X=Zn, Ga, or Al$ ).

### **1.5 Research Questions**

The research intends to answer the following questions:

- i. Based on fundamental principles, what are the electronic structure properties of hexagonal antiperovskite materials  $XCCr_3$  ( $X=Zn, Ga, or Al$ ) and how do they compare to previous works?
- ii. According to the first principles technique, what are the elastic properties of  $XCCr_3$  ( $X=Zn, Ga, or Al$ )?
- iii. According to the first principles technique, what are the superconducting properties of hexagonal antiperovskite materials  $XCCr_3$  ( $X=Zn, Ga, or Al$ )?
- iv. Using a density functional theory method, what are the thermodynamic properties of the materials  $XCCr_3$  ( $X=Zn, Ga, or Al$ )?

### **1.6 Justification of the Study**

Density functional theory is used to measure and calculate the fundamental properties of certain materials such as their crystal structure, electronic structure, and superconductivity properties. Electron density can be easily understood and measured

(Göpel *et al.*, 1984). The quantum mechanical properties of materials at their ground state have been successfully determined using DFT. Based on the study; antiperovskites based on chromium are moderate coupling superconductors. Furthermore, it is anticipated that the study's findings would advance knowledge of chromium-based antiperovskite materials.

### **1.7 Significance of the Study**

Over the years, computational simulations have been employed in the research of materials' properties, including the investigation of their mechanical and electronic properties. Predicting the superconducting properties of  $XCCr_3$  (X=Zn, Ga, or Al) antiperovskite materials was the aim of this research.

### **1.8 Scope of the Study**

First principle-based computational methods were used to collect the elastic, electronic, superconducting, and thermodynamic data of the chromium-based Antiperovskite material. No experimental measurements were performed.

### **1.9 Assumptions**

The assumptions made were:

- i. The required properties could be determined using DFT tools.
- ii. Studies on antiperovskite, a chromium-based compound with a hexagonal crystal structure, and other related topics would be easily accessible.
- iii. The amount of time needed to complete the study would be sufficient to provide the intended outcomes, which would provide answers to the specific objectives.

## CHAPTER TWO

### LITERATURE REVIEW

#### 2.1 Introduction

Properties regarding antiperovskites materials which lead to their superconductivity are covered in this chapter. The conceptual framework is presented and discussed.

#### 2.2 Electronic Structure Properties of Hexagonal Antiperovskite Material

The main area of complexity is the consideration of electron-electron interactions; the interaction of electrons with atomic nuclei and each other determines many of a system's physical and chemical properties. Approximation is necessary in order to readily separate out or address these interactions. The numerical solutions and electronic structure calculations of the Schrödinger equation on a specific system set themselves against other approaches used in modeling since they are based on basic laws (Mollah, 2004). The computation includes the description of the system and not external parameters, as selected by the researcher (Gill *et al.*, 1992). Such computations allow for the study of a system without the need for actual experimentation. The numerical solution of the Schrödinger problem is still challenging.

The exact solutions to the equation can only be found when system size increases exponentially. Other than the lowest and most basic of systems, such as the hydrogen atom, this scaling makes it impossible to do precise calculations. To make the equations easier to solve, approximations may be used, but this comes at the cost of some accuracy and predictive capacity being lost. The most powerful electronic structure techniques today are computational chemistry and density functional theory, which has been utilized for analyzing broad variety in systems with practical applications (Baerends *et al.*, 1973). Possible precision is constrained by assumptions made for the electron-electron interactions in the density functional and quantum chemical techniques (Delft, 2012).

First-principles analyses of the formation energies reveal that the nonmagnetic  $ACr_3$  ( $A = Al$  and  $Ga$ ) materials may be produced at ambient pressure. The band structures demonstrate the metallic character of the materials (Shao *et al.*, 2014).

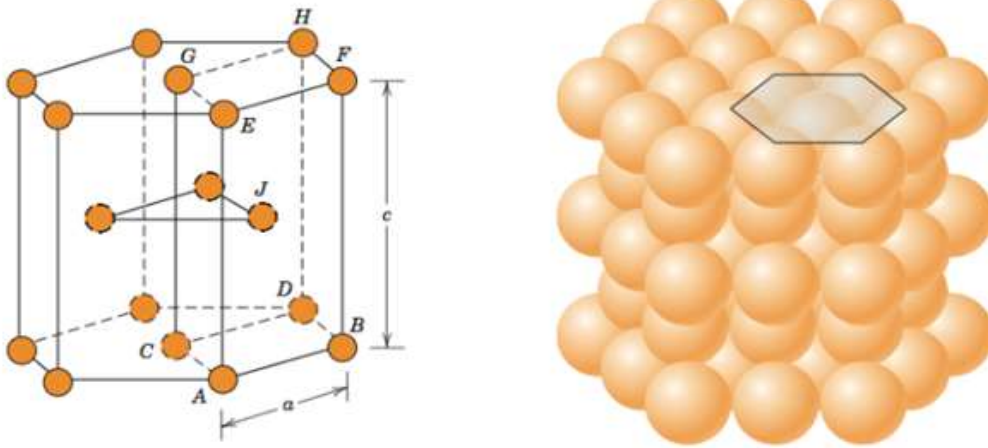
$AsNMg_3$  and  $SbNMg_3$  were studied utilizing the Generalized Gradient Approach, which revealed that they had a narrow band gap and exhibit ionic semiconducting behavior. In contrast to  $SbNMg_3$ ,  $AsNMg_3$  exhibits an indirect band gap (Wright *et al.*, 2014).

$PbNCa_3$  is a metallic substance, whereas  $BiNCa_3$  is a semiconductor with a small band gap. Since lead contains one less electron than bismuth and  $BiNCa_3$  has a relatively narrow band gap, it was predicted that  $PbNCa_3$  would be a metal.  $BiNCa_3$ 's component elements' valences provide an ionic image of the compound, but substantial covalent mixing is also present because of the p-states of Bi and N. The Local Density Approximation (LDA) underestimates band gaps (Papaconstantopoulos & Pickett, 1992). At pressure and room temperature,  $AsNCa_3$  and  $PNCa_3$  crystallize into orthorhombic structures with the  $Pbnm$  group space. The band gap of  $AsNCa_3$  can decrease with pressure as the orthorhombic structure becomes very stable than the cubic structure. At 59 GPa,  $AsNCa_3$  undergoes phase change to the cubic phase, with 15 atoms in a unit cell (Haddadi *et al.*, 2009).

As shown in Figure 1, in a perfect hexagonal halide antiperovskite, the B-site, which is the divalent metal located at the hexagonal body Centre, the anions occupy six face centers, creating octahedral environment for monovalent cations and divalent metal are at the vertices of the hexagon (Wright, 1993).

**Figure 1**

*Unit Cell of Hexagonal Antiperovskite*



*Adapted from Wright, 1993, p. 282.*

### **2.3 Elastic Properties of Hexagonal Antiperovskite**

The system's physical and chemical properties are affected by the way electrons interact with atomic nuclei. Cores are the sites of all three types of interactions between electrons and nuclei. The primary source of problem in establishing these interactions is considering electron-electron interaction when interpreting the properties, since the two interactions are intertwined and can only be treated using approximation. It is possible to tell one system with a properly solved Schrödinger equation apart from another. Time must grow exponentially with system size if these equations are to be solved properly (Hetényi *et al.*, 2001). This scaling renders precise calculations difficult for all but the smallest and most fundamental systems. In order to simplify these equations into a form that can be easily solved, approximations are included, which reduces the degree of accuracy and the predictive ability. Many solutions of the Schrödinger equations can be computed using computer simulation and the density functional theory (DFT) methods, including structural properties, electronic and other material properties that are relevant to a wide variety of systems (Baerends *et al.*, 1973).

The electronic structure properties of cubic antiperovskites were examined by using three distinct computational approaches that is; Generalized Gradient Approximation (GGA), Local Density Approximation (LDA) as well as Engel Vosko. The resulting calculations revealed band-gaps of 0.59 eV for  $\text{SbNCa}_3$  as well as 0.36 eV in  $\text{BiNCa}_3$ , respectively (Mazin *et al.*, 2002). When determining the band structures of these compounds, Engel Vosko-GGA provides higher precision than either LDA or GGA. Despite the fact that EV-GGA created larger band gaps than the experimental findings predicted, these materials nonetheless behave like metals because their valence bands straddle the Fermi level (Moakafi *et al.*, 2009).

Based on the investigation conducted using the full potential augmented plane waves and local orbital (APW + lo) approach, it has been shown that  $\text{AsNMg}_3$  and  $\text{SbNMg}_3$  exhibit small band gaps when considering their structural, electronic and optical properties. Nevertheless, it is worth noting that the band gaps estimated by DFT often exhibit a tendency to underestimate their actual values (Okoye, 2006). Consequently, the computed locations of the optical spectrum could be lower in comparison to the values obtained by experimental measurements. In comparison to  $\text{SbNMg}_3$ , which experiences a shift from an indirect to a direct band gap characteristic at a pressure of 6.85 GPa,  $\text{AsNMg}_3$  retains its direct band gap attribute throughout the entire range of applied pressure. Additionally,  $\text{AsNMg}_3$  exhibits a fundamental direct band gap that initially rises as much as 4 GPa, but subsequently decreases as it reaches higher pressure (Pugh, 1954).

In their study, (Amara *et al.*, 2013) employed the full-potential augmented plane wave along with local orbital method to analyze the density of states, band structure as well as charge density of  $\text{PNMg}_3$ ,  $\text{AsNMg}_3$ ,  $\text{SbNMg}_3$ , and  $\text{BiNMg}_3$ . The investigation also considered the influence of exchange as well as interactions by utilizing the Tran-Blaha



modified Becke-Johnson (mBJ) potential (Amara *et al.*, 2013). Based on the findings of this study, it may be concluded that these compounds exhibit properties of semiconductors. The materials  $\text{SbNMg}_3$  and  $\text{BiNMg}_3$  were identified as examples of indirectly band gap materials, whereas  $\text{PNMg}_3$  and  $\text{AsNMg}_3$  were identified as examples of the direct band gap compounds. When compared to previous studies, the band gap values obtained with the mBJ potential are the greatest.  $\text{PNMg}_3$  has the highest elastic properties, whereas  $\text{BiNMg}_3$  has the lowest. When transitioning from  $\text{BiNMg}_3$  to  $\text{PNMg}_3$ , the covalent nature of these materials becomes more prominent (Tran *et al.*, 2007).

## 2.4 Superconductivity Properties

$\text{GaNCr}_3$  and  $\text{RhNCr}_3$  materials' band structures demonstrate their metallic character (Wiendlocha *et al.*, 2007). Both compounds have a non-ferromagnetic ground state according to spin polarized calculations. These materials' high values for the electronic component of the electron-phonon coupling constant may explain their potential for superconductivity. Below 17K, the cubic antiperovskite  $\text{RhNCr}_3$  material is metallic and superconducting. Its superconductivity's process is not entirely understood (Wright *et al.*, 2014).  $\text{ZnCNi}_3$  was shown to be superconducting at 2K. Mg is deficient from the  $\text{ZnCNi}_3$  material hence the absence of superconductivity (Johannes & Pickett, 2004).

The occupied highest energy states in  $\text{MNNi}_3$  (M = Zn, Mg, or Cd) are characterized by hybridizations involving Nickel-3d and Nitrogen- 2p orbitals in close proximity to the Fermi level, with very little contribution from the M elements (Sieberer *et al.*, 2007). Superconductivity in  $\text{ZnNNi}_3$  was obtained at a temperature of 3K, but none of the other two compounds exhibited this property. The observed phenomenon may be attributed to a marginal augmentation of M variables, resulting in a little displacement of the energy bands in close proximity to the Fermi level (Li *et al.*, 2009).

MgCNi<sub>3</sub>, which is the initial reversed Perovskite superconductor to have been identified, has gained considerable recognition due to its unique property of exhibiting imaginary frequencies (Dolgov et al., 2008). Due to the perpendicular migration of 2 Nickel atoms towards the octahedral, the acoustic mode of the perovskite structure is unstable. In addition, they found that inharmonic effects stabilize this mode, which, when included into the whole investigation, leads to an unusually high calculated  $\mu^* = 1.5154$ . The authors used a rather large scaling factor of  $\mu^* = 0.33$  in order to reconcile this outcome with the experimentally observed transition temperature of 8K. It is possible to find imaginary frequencies by LDA calculations. While producing a critical temperature that is very close to the experimental value (with a standard  $\mu^* = 0.1$ ), the system is dynamically stable for the PBE. Comprehending this outcome may be facilitated by examining its phonon dispersion. In actuality, the PBE possesses a very weak phonon mode that vanishes into thin air when paired with the LDA (Allen & Dynes, 1975). Since the system is so near to the phase transition, even little adjustments to the functional or pseudopotential calculation parameters may have profound impacts (He *et al.*, 2001).

## 2.5 Thermodynamic Properties

The evaluation of thermodynamic properties under temperature offers critical information on chemical stability, which is required for the identification of these materials in order to utilize them effectively in the industrial sector (Li *et al.*, 2009). Because a previous work discovered that pressure has no effect on the changes of entropy and heat capacity with respect to temperature (Johannes & Pickett, 2004). The thermodynamic properties were calculated at zero pressure.

Since energy generation based on thermoelectric offers a potential answer to the twenty-first-century energy dilemma due to the fact that this method does not rely on fossil fuels

and is thus ecologically beneficial, antiperovskites materials have become materials of interest in the thermoelectric industry since thermoelectric materials are used in thermoelectric generators to convert heat to electricity and vice versa (Togo & Tanaka, 2015). Aside from producing electrical energy, thermoelectric technology also minimize thermal pollution caused by the presence of surplus heat in the environment (Ennassiri *et al.*, 2018). The effectiveness of energy conversion is greatly dependent on the type of thermoelectric materials utilized (Wiendlocha *et al.*, 2007).

## **2.6 Research Gaps**

Numerous investigations on the superconductivity of antiperovskite materials have been done. However, many researchers examined the mechanical and electronic properties differently and were unable to make a connection with the materials' superconductivity. The band structures of the materials  $\text{GaNCr}_3$  and  $\text{RhNCr}_3$  indicate that both materials are metallic in. From spin polarized calculations, the ground states of both compounds are non-ferromagnetic. It has been suggested that the presence of superconductivity in these materials can be deduced from the substantial magnitudes of the electron-phonon coupling constant's electronic component. However, the properties were not linked to superconductivity in this investigation.

## 2.7 Conceptual Framework

**Figure 2**

*Conceptual Framework*

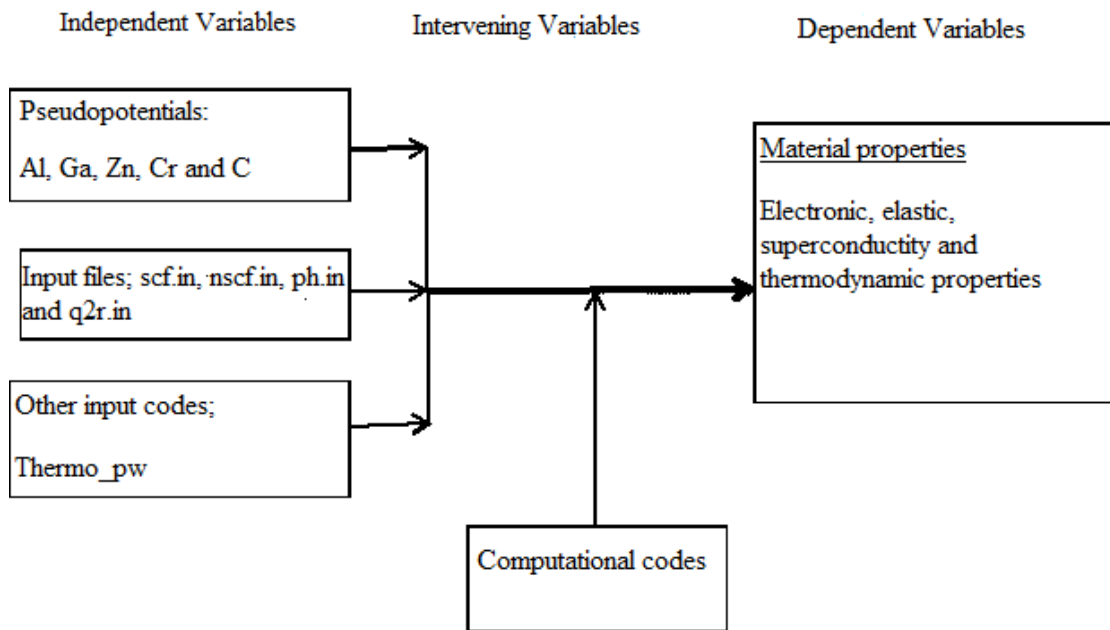


Figure 2 illustrates the proposed conceptual framework. The sets of variable are three: the dependent, independent and intervening variables. The independent variables are pseudopotentials, input files and Thermo\_pw code. The dependent variables are electronic, elastic, superconductivity and thermodynamic properties while computational codes are the intervening variables.

## CHAPTER THREE

### RESEARCH DESIGN AND METHODOLOGY

#### 3.1 Introduction

In the present research, density functional theory was implemented. Using computational methods, several of the key materials were investigated rather precisely. This study aimed to fill the need in the industry for rapid and affordable methods of materials analysis. The computations in this study were conducted utilizing the Quantum Espresso computational software, renowned for its versatility in doing ab initio simulations of periodic as well as disordered condensed matter problems (Singh & Mazin, 2001). The technique of Density Functional Theory (DFT) can be employed to characterize a diverse array of materials, encompassing crystalline solids, molecules, as well as surfaces. Due to the codes ability to operate on a variety of platforms, including straightforward stand-alone machines, calculations were performed in this study on both parallel and serial processors. The properties of matter are described via computational modeling, which is based on equations. Running computer programs written in quantum espresso code enables computer simulation (H.-S. Lee et al., 2007).

Vanderbilt ultrasoft pseudopotentials were used to determine electron-ion potential. The rapid optimization of the expected cut off energy and features of the system is attributed by the smooth and transferable properties of the ultrasoft pseudopotentials method, particularly in relation to the development of the plane wave basis set. In electronic structure simulations, the PBE version of the GGA pseudopotential was used to account for exchange as well as correlation energy (Prokopenko *et al.*, 2019)

#### 3.2 Description of the Working of Quantum Espresso

Modelling and first-principles computation are the primary goals of the Fortran-based quantum espresso software was utilized to investigate and develop the electronic

structure using simulation and optimization techniques, employing Density Functional Theory (DFT), waves with planes basis sets, and pseudopotentials(Mackenzie & Maeno, 2003). The Quantum Espresso functions pertaining to the plane wave density functional theory were derived by means of the plane-wave self-consistent field (PWscf), a collection of software tools designed to calculate electronic structures properties (Gordon *et al.*, 2013).

Computational packages were employed to iteratively solve the self-consistent Kohn-Sham equations for a periodic structure. The obtained results were afterwards utilized for the purpose of data analysis and visualization. Quantum Espresso employs ground-state energy and one-electron Kohn-Sham orbitals to estimate atomic forces, stresses, and optimum structure. To obtain the band structure and optimize K points, Cutoff energy, and symmetry points, the data executes programs of scf, nscf, and bands calculations. PWscf modules pw.x and ph.x for input data and pp.x for post processing are supported by the program.

The scripts for data post processing in pp.x retrieve the desired data from files created by pw.x, and then they prepare the data for plotting by putting them into forms that the plotting programs can read. Many of these programs end in ".x," such as Bands.x, Plotband.x, Dos.x, Ph.x, and Lambda.x. Band structure visualization from the bands.x files that were extracted by pw.x.plotband.x used the output from bands.x, which was generated when dos.x calculated the Density of States (DOS), and used it to draw charts depicting various band topologies. While ph.x determined phonon dispersion, Lambda.x computed the superconducting transition temperature.

### 3.3 Electronic Structure Properties

The corresponding Perdew-Burke-Ernzerhof (PBE) Norm preserving pseudopotentials were used for all density functional theory computations. The ground-state ab-initio calculations properties have been effectively used the density functional theory (Gonze *et al.*, 2002). In light of these considerations, the investigation was conducted with the plane wave self-consistent field (PWscf) technique, which was implemented within the Quantum Espresso software package. The results are comparable to those obtained using other all-electron techniques. The successful achievement of the optimization of the energy at the lowest ecut threshold was attained by the utilization of appropriate basis sets. Graphing was employed for verification of the correct cell size, k-point, and kinetic energy threshold values. The lattice constants for structural properties were calculated using the Murnaghan equation of state and the energy volume relation (Murnaghan, 1944). Dimensions of a unit cell, in essence when one material's lattice constant is different from another, stresses are introduced into the layer, preventing the epitaxial development of larger layers without defects. The density of state is calculated as a byproduct of computing the electronic structure using the necessary K-mesh, and the band structure was computed after structural optimization of non-self-consistent fields was performed with the input file's atomic positions left unchanged.

The phonon band and PHDOS curves are calculated and plotted for all the three materials to provide information about the lattice dynamic properties. Both materials phonon dispersion curves and phonon– DOS were estimated along the high symmetry points ( $\Gamma$ -X-K- $\Gamma$ -L-W-X) of the Brillouin zone. Because there are no imaginary phonon frequencies, the materials were dynamically stable.

### 3.4 Elastic Properties

Most of a compound's structural, thermal, and mechanical behaviors are determined by its elastic properties. Furthermore, elastic properties provide further information about how a particular material responds to external forces applied to the crystal. The thermo-pw code was used to calculate the elastic constants, and the strains were induced to the primitive vectors of the unstrained structures. The strain energy was determined by calculating the whole set of elastic constants, which enables the determination of shear modulus, Young's modulus as well as Poisson's ratio for all crystallographic orientations (Kamihara *et al.*, 2008). This analysis aims to evaluate the presence of anisotropy in these materials. In our computations, the value of *ecutrho* was chosen as 720 Ry, while the wave functions cut-off of the kinetic energy was fixed at 35 Rydberg. The parameters used for the smearing width, convergence threshold and mixing beta were all set at 0.01 Ry, 1.0 E-12 Ry, and 0.4 Ry, respectively. Each compound has a K-point split of 18×18×4. XcrysDen was used to examine the, while Linux was employed as the operating system. Both Xmgrace and GNU plot were used to create the visuals (Shim *et al.*, 2001). The Bravais lattice vector of the hexagonal phase is given by;

$$C_{ij} = \begin{bmatrix} C_{11} & C_{12} & C_{13} & 0 & 0 & 0 \\ & C_{11} & C_{13} & 0 & 0 & 0 \\ & & C_{33} & 0 & 0 & 0 \\ & & & C_{44} & 0 & 0 \\ & & & & C_{44} & 0 \\ & & & & & X \end{bmatrix} \quad \dots (3.1)$$

Where,  $X = \frac{1}{2}(C_{11} - C_{12})$ . The matrix in (3.1) has a symmetric leading diagonal. The strain energy of hexagonal class crystals is constituted by 5 distinct elastic constants, which includes  $C_{11}, C_{12}, C_{13}, C_{33}$  and  $C_{44}$  (Nyawere *et al.*, 2014). A tetragonal crystal's defining feature, element X, is instead derived from another relation in the matrix  $C_{ij}$ .



Limits of Voigt and Reuss types are calculated for both the bulk and shear moduli (Nye & Lindsay, 1957). The elastic constants can be derived from energy fluctuations by applying a little amount of strain to the convergent lattice structure provided by;

$$B = \frac{1}{3}(C_{11} + 2C_{12}) \quad \dots (3.2)$$

$$G = \frac{1}{5}(3C_{44} + C_{11} - C_{12}) \quad \dots (3.3)$$

Equations (3.4) and (3.5) offer the Voigt limits of  $B_V$  and  $G_V$ , while Voigt-Reuss-Hill (VRH) provides approximations for the shear and bulk moduli (Davaranah et al., 2020).

$$B_V = \frac{2}{9}(C_{11} + C_{12} + \frac{1}{2}C_{33} + 2C_{33}) \quad \dots (3.4)$$

$$G_V = \frac{1}{30}(7C_{11} - 5C_{12} + 12C_{44} + 2C_{33} - 4C_{13}) \quad \dots (3.5)$$

Moreover, the Reuss limits are given by;

$$B_R = \frac{C_{33}(C_{11} + C_{12}) - 2C_{13}^2}{C_{11} + 2C_{33} + C_{12} - 4C_{13}} \quad \dots (3.6)$$

$$G_R = 2 \frac{1}{2} \frac{[(C_{11} + C_{12})C_{33} - 2C_{13}^2]C_{44}C_{66}}{3B_V C_{44} + [(C_{11} + C_{12})C_{33} - 2C_{13}^2](C_{44} + C_{66})} \quad \dots (3.7)$$

Using VRH, B and G are expressed as

$$B_{VRH} = \frac{1}{2}(B_V + B_R) \quad \dots (3.8)$$

$$G_{VRH} = \frac{1}{2}(G_V + G_R) \quad \dots (3.9)$$

The Voigt and Reuss versions are indicated by the subscripts  $V$  and  $R$ , respectively (Kohn & Sham, 1965). The values of  $E$  and  $\nu$  are given by;

$$E = \frac{9BG}{3B + G} \quad \dots (3.10)$$

$$\nu = \frac{3B - 2G}{2(3B + G)} \quad \dots (3.11)$$

Three shear-type anisotropy ratios, denoted by the letters  $A_1$ ,  $A_2$ , and  $A_3$ , are present in hexagonal crystals.

$$A_1 = \frac{\frac{1}{6}(C_{11} + C_{12} + 2C_{33} - 4C_{13})}{C_{44}} \quad \dots (3.12)$$

$$A_2 = \frac{2c_{44}}{(c_{11} - c_{12})} \quad \dots (3.13)$$

And

$$A_3 = A_1 A_2 \frac{\frac{1}{3}(C_{11} + C_{12} + 2C_{33} - 4C_{13})}{C_{11} - C_{12}} \quad \dots (3.14)$$

One of the common approaches to calculating the Debye temperature is to estimate it from the mean sound velocity ( $V_M$ ) using equation (3.15)

$$\Theta_D = \frac{\hbar}{k_B} \left[ \frac{3nN_{A\rho}}{4\pi M} \right]^{-1/3} V_M \quad \dots (3.15)$$

In this context, the symbol " $\hbar$ " denotes the Planck constant, " $k_B$ " symbolizes the Boltzmann constant, " $N_A$ " signifies Avogadro's number, and " $V_M$ " denotes the mean speed of sound in air (Ortenzi *et al.*, 2011). An approximation of the formula for the mean speed of sound is as follows:

$$V_m = \left[ \frac{1}{3} \left( \frac{2}{\nu_l^3} + \frac{1}{\nu_t^3} \right) \right]^{-1/3} \quad \dots (3.16)$$

The bulk modulus  $B$  and the shear modulus  $G$  may be used to calculate the longitudinal sound velocity, indicated as  $\nu_l$ , and the transverse sound velocity, denoted as  $\nu_t$ .

$$V_l = \left( \frac{3B + 4G}{3\rho} \right)^{1/2} \quad \dots (3.17)$$

$$V_t = \left( \frac{G}{\rho} \right)^{1/2} \quad \dots (3.18)$$

### 3.5 Superconductivity Properties

Established techniques were combined with more recent machine-learning techniques. The electron-phonon spectra were computed using density functional perturbation theory. Machine learning approaches are employed to not only make predictions, but also to comprehend significant physical factors, namely the strength of electron-phonon coupling ( $\lambda$ ) as well as the average frequency of phonons  $\omega_{ln}$  (Wälte *et al.*, 2004). In practice, materials close to structural instabilities, or those with a high electron-phonon coupling constant, exhibit some anti-correlation between ( $\lambda$ ) and  $\omega_{ln}$ . This is especially true for soft phonon systems. The expected monotonic, but non-linear, growth in  $\omega_{ln}$  with increasing pressure holds. After finding that transitional temperature decreases with pressure up to approximately 15 GPa, it rises to a maximum of around 5.4 K at 55 GPa. The conducted comprehensive high-throughput search showed that AlCCr<sub>3</sub> had the highest superconducting transition temperature of the three material tested.

The Perdew-Wang local-density approximation was employed in the computation regarding superconducting properties (Perdew & Wang, 1992). A conventional grid with dimensions of 6×6×1 was employed for the q-sampling on the phonons, which is consistent with previous theoretical research on inverted Perovskite (Ma *et al.*, 2019). Using dense 8×8×8 q-point grid, the calculations were run to determine the sampling quality (Savrasov, 1996). The values of  $\lambda$  and  $\omega_{ln}$  were subsequently employed in the computation of the superconducting transition temperature.

$$\lambda = 2 \int \frac{a^2 F(\omega)}{\omega} d\omega \quad \dots (3. 19)$$

The value of  $\mu^*$  for transition metals ranges from 0.1 to 0.2. The value can be obtained by utilizing a modified version that uses the Bennemann-Garland empirical equation, which considers the estimated density of states at the level of Fermi (Bennemann & Garland, 1973).

$$\mu^* = \frac{0.26N(E_f)}{(1 + N(E_f))} \quad \dots (3. 20)$$

The logarithmic average phonon frequency ( $\omega_{\ln}$ ) using is given by;

$$\omega_{\ln} = \exp(2\lambda^{-1} \int_0^\infty \frac{d\omega}{\omega} a^2 F(\omega) \ln \omega) \quad \dots (3. 21)$$

The phonons in a crystal lattice can be used to explain a material's strength (Agora et al., 2022). The vibration modes serve to mitigate the stresses experienced by the atoms displaced from their state of equilibrium due to symmetry. As a result, their oscillation's frequency is likewise reduced. The outcome is a decrease in crystal energy and a negative energy distribution to the soft phonons as a result of periodic lattice distortions caused by the effect. In this instance, the phonon frequencies will serve as the criterion for the stability of the crystal, and depending on their magnitude, instability may develop. The electron-phonon properties are computed utilizing the density functional perturbation theory. Previous studies have shown instances of superconductivity among antiperovskite carbides, nitrides, as well as phosphides (Bennemann & Garland, 1973). The phenomenon of superconductivity in compounds with conventional valence states can be linked to the regular pairing of transition atoms  $d$  electrons, facilitated by phonons (He *et al.*, 2001). A  $4 \times 4 \times 4$  q-point grid was used for phonon computations on each structure to sample the Brillouin zone. For the EPC computations, a denser  $12 \times 12 \times 12$  q-point grid was employed. Fourier interpolation was utilized to determine phonons for

every selected q-point after the dynamical matrices were constructed on a  $4 \times 4 \times 4$  grid. Understanding material properties like thermal and electrical conductivity is aided by phonon research. A phonon is a particular type of crystal lattice vibration in which all of the particles vibrate at the same particular frequency (Koretsune & Arita, 2017). A dispersion relation is the correlation between the wave vector and the frequency of vibration, and it is as follows:

$$\omega = v(k) \quad \dots (3. 22)$$

In this context, the symbol  $k$  represents the wave vector, symbol  $\omega$  represents the vibration frequency, and symbol  $c$  represents the sound velocity. Temperature at which transition occurs was determined using the McMillan equation, which was created from the Eilenberg theory inside the BCS theory and is represented by equation 3.23 (Dynes, 1972).

$$T_c = \frac{\theta_D}{1.45} \exp \left[ \frac{-1.04(1 + \lambda)}{\lambda - u^*(1 + 0.62\lambda)} \right] \quad \dots (3. 23)$$

The renormalized Coulomb repulsion, denoted as  $u^*$ , is assigned a value within the range of 0.1 to 0.2 (Bennemann & Garland, 1973).

### 3.6 Thermodynamic Properties

The knowledge of the entire phonon spectrum granted by DFPT makes possible the calculation of several important thermo-dynamical properties as functions of temperature  $T$ . In this research, the phonon contribution to the Helmholtz free energy  $\Delta F$ , the phonon contribution to the internal energy  $\Delta E$ , the entropy  $S$ , and the constant-volume specific heat  $C_v$ , at temperature  $T$ , are calculated within the harmonic approximation (H.-S. Lee et al., 2007). In relation to a solid medium, the propagation of sound is characterized by the presence of two transverse waves together with a longitudinal wave (Wu *et al.*, 1987). This phenomenon can be mathematically represented as;

$$\text{total number of states} = 3g(\omega)d\omega \quad \dots (3.24)$$

$$\text{phonon energy} = \frac{1}{\exp\left(\frac{h\omega}{K_B T}\right) - 1} \quad \dots (3.25)$$

$$\text{number of modes} = E = \frac{3\nu}{2\pi^2\nu^3} \int_0^{\max} \frac{h\omega^3}{\exp\left(\frac{h\omega}{K_B T}\right) - 1} \quad \dots (3.26)$$

let  $x = \left(\frac{h\omega}{K_B T}\right)$  and Debye Temperature;  $\theta = \frac{h\omega_{\max}}{K_B}$

Equation (3.26) has the following form:

$$E = \frac{3\nu K_B T^4}{2\pi^2\nu^3 h^3} \int_0^{\theta_D/T} \frac{x^3}{\exp(x) - 1} \quad \dots (3.27)$$

Debye model heat energy is defined by equation (3.27).

At Low temperature;

$$\text{Taking limits} \int_0^{\infty} \frac{x^3}{\exp(x) - 1} dx = \frac{\pi^4}{15}$$

Debye heat capacity is defined as;

$$C = \frac{dE}{dT} = \frac{12\pi^4}{5} NK_B \left(\frac{T}{\theta_D}\right)^3 \quad \dots (3.28)$$

Equation (3.28) represents the Debye model's low-temperature specific heat capacity.

At high Temperature;

Due to the fact that  $x$  is small;

$$\exp(x) \approx 1 + x$$

$$\int_0^{\theta_D/T} \frac{x^3}{1 + x + \dots} - 1 dx \approx \frac{\theta_D}{3T^3} \quad \dots (3.29)$$

$$E = \frac{\nu K_B^4 T \theta_D^3}{2\pi^2\nu^3 h^3} \quad \dots (3.30)$$

And since;

$$\nu = \frac{\theta_D K_B}{h} \left( 6\pi^2 \frac{N}{V} \right)^{-1/3}$$

Equation (3.30) therefore becomes;

$$E = 3NK_B T \quad \dots (3.31)$$

Debye heat capacity at high temperature becomes

$$C = \frac{dE}{dT} = 3NK_B \quad \dots (3.32)$$

Where  $k_B$  is the Boltzmann constant,  $n$  is the number of atoms per unit cell,  $N$  is the number of unit cells,  $\omega$  is the phonon frequency,  $\omega_{max}$  is the largest phonon frequency

and  $g(\omega)$  is the normalized phonon density of states with  $\int_0^{\omega_{max}} g(\omega) d\omega = 1$ . Debye's

specific heat capacity at low temperatures is represented by equation (3.28) and at high temperatures by equation (3.32).

### 3.7 Derivation of the Governing Equations and Theorems

The simulation is based on the Schrödinger equation's solution, the Density Functional Theorem, Born-Oppenheimer Approximations as well as Kohn-Sham Equations. The most effective and popular ab-initio approach is DFT (Gross & Dreizler, 1976). The foundation of this approach is in the Hohenberg- Kohn theorem, which suggests that the properties of the ground state of an electron gas with spatial variations can be described by a functional dependent on the electron density (Kohn & Sham, 1965).

#### 3.7.1 The Many Body Problem

The equation developed by Schrödinger serves as the fundamental basis for conducting quantitative analyses of the properties exhibited by solid state materials. It is widely accepted that the Hamiltonian of the system is typically composed of the aggregate of the

system's particles' kinetic energy, denoted as  $T$ , and the summation of the energy resulting from electron-nucleus interactions, referred to as potential  $V$ . The effectiveness of computational methodologies can be attributed to the initial conversion of Schrödinger equation into Kohn-Sham equations, as well as the scientific comprehension of the correlation effects exhibited by interacting electrons in the presence of a gradually changing field. The solution of the Kohn-Sham equations can be easily obtained. A perspective on solids involves conceptualizing them as an assemblage of positively charged ion cores that are suspended within a surrounding medium composed of valence electrons. The electronic properties of a small, self-contained system consisting of  $N$  interacting electrons, subject to an external potential, exhibit similarities to the electronic properties of the system when it is in its lowest energy state.

The external potential generated by an arrangement of atomic nuclei is traditionally conceptualized as originating from a fixed point of electrons. The ionized centers are comprised of the atomic nucleus and the electrons in the innermost orbitals, which are fully occupied. The core may be seen as a classical particle since it is so massive and moves so much slower than electrons. However, due to their diminutive size and rapid motion, valence electrons must be categorized as quantum particles. Only the valence electron contributes to reactions and forms bonds between atoms in a solid (Jha, 2005).

The generic Hamiltonian of the many-body system can be expressed as;

$$H = \sum_i -\frac{\hbar^2}{2M_i} \nabla_i^2 + \frac{1}{2} \sum_{i,j} \frac{z_i z_j e^2}{(R_i - R_j)} - \sum_k \frac{\hbar^2}{2M_e} \nabla_{rk}^2 + \frac{1}{2} \sum_{kl} \frac{e^2}{r_k - r_l} \sum_{ki} \frac{z e^2}{r_k - R_l} \dots (3.33)$$

Where;

$M_i$  = nuclear mass at the  $R$  location

$M_e$  = The total weight of an atom situated at location  $r_i$

$Z$  = represents the mass number of an element.



Equation (3.33) can be concisely expressed as.

$$H = T_e + T_n + W_{ee} + W_{en} + W_{nn} \quad \dots (3. 34)$$

The electron and nuclear kinetic energies are represented by the first two components in the equation above, while the electron-electron, electron-nucleus, and nucleus-nucleus interactions are represented by the remaining three terms. The preceding equation cannot be solved due to the system's large number of independent variables (Turquette, 1958). The issue may be resolved by using Born Oppenheimer's adiabatic approximation. Due to the Bohn-Oppenheimer approximation, the nucleus has a mass that is significantly more than the electronic mass and travels more slowly than the electrons. The motion of the ions and electrons may be investigated separately from the adiabatic approximation. One function that describes the electrons and another that describes the ions can be combined to create the system's overall wave function (Cederbaum, 2004).

$$\varphi_v(r_i, R_a) = \theta(r_i, R_a) \chi(R_a) \quad \dots (3. 35)$$

All of the interactions between the electron and the nuclei are taken into account by the Schrödinger equation. The system still has  $10^{23}$  degrees of freedom and is hence complicated even if the issue has been broken down into an electronic component and an ionic component. In the context of the quantum many-body problem, it is conventionally thought that  $W_{en}$  represents the external potential, whereas  $W_{nn}$  is treated as a constant. However, a complication occurs with respect to  $W_{ee}$ , as the collective wave function encompassing all electrons is contingent upon their respective coordinates, making it impossible to separate the issue into a single particle problem. The interaction of the electrons is what causes this. Further developments are required in order to do computations on an actual system as a result of this issue. Density functional theory (DFT) has been used as a strategy to deal with electron density, which is a variable

characterized by three coordinates. Unlike wave functions that depend on electron coordinates, DFT utilizes electron density to tackle this problem (Wright *et al.*, 2014).

### 3.7.2 Electronic Density

Let  $N$  represent the total quantity of electrons and  $r_i$  denote the position of electron  $i$ , along with its spin coordinate,  $\sigma_i = \uparrow$  or  $\downarrow$  (Papaconstantopoulos & Pickett, 1992). Wave function of a multi-electron system, which is contingent upon the spatial and spin coordinates  $\psi_e(r_1\sigma_1, r_2\sigma_2, \dots, r_N\sigma_N)$ , elucidates the quantum mechanical phenomena exhibited by the system. Based on the two specified criteria, the wave function in question has been deemed genuine (Vaghela *et al.*, 2022). Prior to any further analysis or processing, it is necessary to first normalize the data;

$$\langle \Psi_e | \Psi_e \rangle = \sum_{\sigma_1, \dots, \sigma_N} \int dr_1 \int dr_2 \dots \int dr_N |\psi_e(r_1\sigma_1, r_2\sigma_2, \dots, r_N\sigma_N)|^2 = 1 \quad \dots (3.36)$$

Additionally, it is necessary for it to exhibit anti-symmetry;

$$\psi_e(\dots, r_i\sigma_i \dots r_j\sigma_j \dots) = -\psi_e(\dots, r_j\sigma_j \dots r_i\sigma_i \dots) \quad \dots (3.37)$$

The electron density, denoted as  $n(r)$ , represents the quantity of electrons per unit volume at a specific place  $r$  within an electronic system (Vaghela *et al.*, 2022). The equation representing the overall quantity of protons is as follows:

$$\int n(r) d^3r = N \quad \dots (3.38)$$

The expression of electron  $n(r)$  can be represented by;

$$n(r) = \sum_{i=1}^N \delta(r - r_i) \quad \dots (3.39)$$

The function  $n(r)$  with multiple electrons is additionally suggested using the equation below;

$$n(r) = N \sum_{\sigma_1, \dots, \sigma_N} \int dr_2 \int dr_3 \dots \int dr_N |\psi_e(r_2\sigma_2, r_3\sigma_3, \dots, r_N\sigma_N)|^2 \quad \dots (3.40)$$

The expression on the right side in equation (3.40) has resemblance to the integration for wave function normalization (3.39), with the exception that it lacks one spatial integral and one coordinate. The calculation of the likelihood of finding an electron with spin in a volume element  $d^3$  at position  $r$  involves integrating the coordinates and spins of the remaining  $(N-1)$  electrons inside the electron density spin  $n(r)$  (Schaak *et al.*, 2004).

$$n_{\sigma}(r) = \frac{1}{N-1} \sum_{\sigma_2, \dots, \sigma_N} \int dr_2 \int d^3 r_2 \dots \int d^3 r_N N! |\psi(r\sigma, r_2\sigma_2, \dots, r_N\sigma_N)|^2 \quad \dots (3.41)$$

The combination of equations (3.40) and (3.41) will result in;

$$\sum_{\sigma} \int dr_{\sigma}(r) = \int (n_{\uparrow}(r) + n_{\downarrow}(r)) = N \quad \dots (3.42)$$

Determining the properties of materials using ab initio method requires that a solution to equation 3.41 is found. However, this equation is extremely difficult to solve numerically due to its huge dimensions, thus, necessitating approximations. The first and most important approximation is the Born-Oppenheimer approximation (BOA) which decouples the dynamics of the nuclei and electrons. Named after Max Born and J. Robert Oppenheimer, BOA allows the electrons and nuclear degrees of freedom to be separated giving room for the wave-function to be broken into its electron and nucleus components. The nucleus and electrons are attracted to each other with the same magnitude of electric charge, and hence they exert the same force and momentum. While exerting the same momentum, the nucleus with a much larger mass in comparison to the electrons will have a very small velocity and considered almost negligible. Thus, the motion of the nucleus is ignored in the solving of the Schrodinger equation. The electrons are much less massive than the nuclei and therefore the electrons will respond almost instantaneously to the movement of the nuclei. Thus, the energy for a given nuclear configuration will be that of the ground state of the electrons in that configuration. In principle, equation 3.42 may be mathematically solved to arbitrary accuracy by

representing it as a direct product wave-function and diagonalizing the Hamiltonian. However, the cost of this calculation scales exponentially with the number of electrons in the system and is intractable for all but the smallest of systems.

### 3.7.3 Hartree-Fock Approximation

In the variation technique, the wave functions for a multi-electron system are expressed as an anti-symmetrized product of a single electron wave function. The approximation being discussed in this context violates the fundamental requirement of the exclusion principle suggested by Pauli which states that, “the many-body wave function must exhibit anti-symmetry when the coordinates of two electrons are interchanged”. The fulfillment of this condition can be achieved through the construction of a Slater determinant including single-particle orbitals (Rosner et al., 2001). In order to ensure compliance with this principle, it is necessary to incorporate the fermionic nature of atoms into a many-body wave function. This is particularly important when utilizing the Hartree wave function approximation, which does not inherently obey the aforementioned principle (Turquette, 1958). When the spatial coordinates of two electrons are interchanged, the resulting wave function exhibits a change in its sign. The mathematical expression for the Hartree-Fock wave function is expressed by the following formula:

$$v_i^{HF}(r) = e^2 \int \frac{n(r') - n_i^{HF}(r, r')}{|r - r'|} dr' \quad \dots (3.43)$$

This technique is frequently employed in chemistry and is reliable for systems with few electrons. The Hartree-Fock approximation, which has resemblance on the standard single-electron model of electronic structure, posits that the distribution of  $N$  electrons is solely determined by the aggregate of all the one-electron distributions  $|\psi^2|$  (Bardeen *et al.*, 1957). It is important to remember that this is only a side effect of the original ansatz

and that in certain situations, modifications to notions like labeling electrons according to angular momenta are essential (Vaghela *et al.*, 2022).

By assuming a wave function with a single determinant, the Hartree-Fock theory ignores electron correlation. Describing the electronic structure accurately becomes difficult when the charged particles are subjected to a mean non-local potential resulting from the presence additional electrons. Although qualitatively correct, Hartree-Fock theory lacks the precision to offer quantitative predictions for many materials and compounds. The Hartree-Fock approximation corresponds to the conventional single-electron picture of electronic structure. This allows concepts such as labelling of electrons by angular momenta. Hartree-Fock theory by assuming a single-determinant form for the wave-function, neglects correlation between electrons. The electrons are subject to an average non-local potential arising from the other electrons which can lead to a poor description of the electronic structure. Although qualitatively correct in many materials and compounds, Hartree-Fock theory is insufficiently accurate to make accurate quantitative predictions. Beyond Hartree-Fock formalism, Hartree-Fock is improved by taking into account the electron correlation.

### **3.8 Density Functional Theory**

It was initially formulated in the 1961 by Hohenberg, Kohn, and Sham, and had a significant increase in prominence during the 1980s. DFT is a popular approach for predicting a material's electronic properties (Manyali *et al.*, 2014). The three variables  $x$ ,  $y$ , and  $z$  are utilized to calculate the electron density, which is then used to calculate ground state properties. The determination of the energy and other properties of a system's ground state is solely reliant on the electron probability density, denoted as  $n(r)$ (Hohenberg & Kohn, 1964).

$$E_{tot} = E[n(r)] \quad \dots (3.44)$$

By incorporating the exchange as well as effects of correlation into the calculation of total energy, the theory effectively addresses the limitations posed by the Hartree-Fock formulation. Correlation illustrates the disparity arising from the total energy of an electronic system as well as the energy of the system as calculated using the Hartree-Fock approximation for an electron gas. On the other hand, exchange denotes the decrease in the energy of the coulomb. The determination of the ground state electronic structure is achieved by the utilization of Density Functional theory as a computational technique. While the practical implementation may lack precision, the theoretical framework remains accurate. Due to its capability to accurately model periodic bulk materials, surfaces, and interfaces, density functional theory is widely favored in the field of materials research. To maximize the use of computational resources, the pseudopotential plane wave technique is frequently used in computations. The anticipated value of every operator is dependent on the charge density. Kohn and Sham demonstrated the feasibility of mapping a many-particle system onto a non-interacting particle system by leveraging the functional relationship between the ground state energy and the ground state charge density. With a great refinement of the approximations used to better model exchange and correlation in 1990s, DFT which was considered inaccurate in the 1970s has evolved to be rather an accurate tool. As a matter of fact, solid-state system calculations agree satisfactorily with experimental data especially on the description of the structural and electronic properties of a vast class of materials. Computationally, DFT is cheaper compared to traditional methods like HF and its descendants based on the complex manyelectron wave-functions. With all these reasons, DFT is a common tool for describing and predicting the properties of the molecular and condensed matter systems. At this point, however, it is worthwhile noting that despite

recent improvements, there are still difficulties in using density functional theory to properly describe intermolecular interactions especially dispersion, charge transfer excitations, transition states, global potential energy surfaces, dopant interactions and some other strongly correlated systems. There is also a limitation in calculation of the band gap (underestimation of the band gap) and Ferro-magnetism in semiconductors. The subsequent sections provide a concise elucidation of the density functional theory.

### 3.8.1 Hohenberg and Kohn Theorem

A strategy to resolve the electronic component of the Schrödinger equation was put out by Hohenberg and Kohn in 1964. The first theorem establishes a relationship between the electron potential and the ground state electron density. Hohenberg and Kohn were able to illustrate a theorem by considering various external potentials,  $V_{\text{ext}}$  and  $V'_{\text{ext}}$ , that give rise to two Hamiltonians,  $H$  and  $H'$ , respectively. They also considered various trial wave functions,  $\psi$  as well as  $\psi'$ , for  $H$  with  $H'$ , respectively. The ground state electron density produced by both is  $E_{GS}$  and is given by equations below;(Hohenberg & Kohn, 1964)

$$E_{GS} < \langle \Psi | H' | \Psi \rangle = \langle \Psi | H | \Psi \rangle + \langle \Psi | H' - H | \Psi \rangle \quad \dots (3.45)$$

$$E'_{GS} < E'_{GS} + \int [v'_{\text{ext}} - v_{\text{ext}}] n(r) d^3 r \quad \dots (3.46)$$

This also implies

$$E_{GS} < E'_{GS} + \int [v_{\text{ext}} - v'_{\text{ext}}] n(r) d^3 r \quad \dots (3.47)$$

Adding equations (3.46) and (3.47), one obtains

$$E'_{GS} + E_{GS} < E_{GS} + E'_{GS} \quad \dots (3.48)$$

This observation provides evidence that it is not feasible for two distinct external potentials to generate an identical electron density. Therefore, in theory, Hamiltonian operator can be uniquely determined given a charge density, allowing us to calculate the

wave function and all other features of a system. Since  $V_{ext}$  and other ground state parameters including total energy,  $E[n(r)]$ , are dictated using the electron density, the energy of an electron density functional may also be described. Everything's energy shows up as;

$$E[n(r)] = T[n(r)] + W_{ee}[n(r)] + V_{ext}[n(r)] = F[n(r)] + \int V_{ext}(r)n(r)dr \quad \dots (3.49)$$

The terms used to represent the kinetic energy possessed by electrons, which are the energy associated with electron-electron interaction, as well as the external potential amongst the particles are indicated as  $T[n(r)]$ ,  $W_{ee}[n(r)]$  as well as  $V_{ext}[n(r)]$ . The discovery of the exact solution to the Schrödinger equation would be possible if its knowledge were available. According to the second theorem, it may be said that for each given trial electron density  $n(r)$ , where  $r$  represents the position vector given by;

$$\int n(r)d^3r = N \quad \dots (3.50)$$

Then;

$$E[n(r)] > E_{GS} \quad \dots (3.51)$$

According to the initial theorem proposed by Hohenberg and Kohn, Hamiltonian and wave function can be uniquely determined by the trial density, denoted as  $n(r)$ . It follows from the variational principle that;

$$E_{GS} = \langle \psi | H | \psi \rangle \geq E_{GS} \quad \dots (3.52)$$

Under the condition that the conservation of electron count is upheld, the ground state energy and density are associated with the functional minimum, denoted as  $E[n(r)]$ . The electronic chemical potential  $\mu$  serves as the Lagrange multiplier for the constraints.

$$E_{GS} = F[n(r)] + \int V_{ext}(r)n(r)dr - \mu[\int n(r)d^3r - N] \quad \dots (3.53)$$



The equation provided above allows for the deduction of the remarkable observation that there exists a general functional, denoted as  $F[n(r)]$ , which remains unaffected by external potential. To get the precise ground state energy and density, this function would need to be known and then it could be added to the equation and reduced (Diener, 1990).

### 3.8.2 The Kohn-Sham equation

The interpretation for exchange-correlation energy,  $E_{xc}$ , revolutionized DFT and made it a useful tool for routine research of material properties. The term "exchange-correlation energy" is used to describe the fraction of the total energy that arises through non-classical electrostatic interaction with the disparity occurring as a result of the true kinetic energy  $T$  as well as the non-interacting kinetic energy  $T_S$ , when these contributions are shown to be insignificant (Hohenberg & Kohn, 1964). To solve this problem using the Hohenberg-Kohn functional, potential  $V^{KS}(r)$  is first created, where the ground state charge density,  $n(r)$  is calculated. Extra system comprising non-interacting electrons that are subject to motion inside an external potential  $V^{KS}$  in the system have been considered, the electron density in the ground state is computed from the orbitals, and it is same as real interacting system with kinetic energy. In the absence of any external influences, the functional can be precisely characterized as;

$$F[n(r)] = T_S[n(r)] = \langle \phi^{KS} | T | \phi^{KS} \rangle \quad \dots (3.54)$$

The expression of the energy functional is presented as;

$$E^{KS}[n(r)] = \min[T_S(n(r)) + \int V^{KS}(r)n(r)dr - \mu'[\int n(r)d^3r - N]] \quad \dots (3.55)$$

The Lagrange multiplier, denoted as  $\mu'$ , takes into account the preservation of the overall electron count. Due to nonlinear nature of this equation, a self-consistent solution is required. The exchange correlation energy, whose explicit form is unknown, presents the biggest obstacle. The exchange and correlation interactions that result from the Coulomb

contact between the electrons are included in the effective potential as well as the external potential (Manyali *et al.*, 2014).

### 3.8.3 Exchange-Correlation Approximation

The functional is expressed in terms of density and is denoted as;

$$E_{xc}(n) = T(n) - T_0(n) + U_{xc} \quad \dots (3.56)$$

Where;

$T(n)$  = the correct kinetic energy functional

$T_0(n)$  = the interaction-free kinetic energy functional

$U_{xc}$  = the electron-hole exchange correlation interaction.

The shape of  $U_{xc}$  cannot be determined easily and hence electron density-based approximation functions are used to provide a working definition. GGA and the LDA functionals are two prominent instances of approximation functional that are extensively employed in various applications.

### 3.8.4 Local Density Approximation (LDA)

The primary concept involves the local approximation of the exchange correlation energy within an interacting electron system by utilizing the exchange-correlation-energy of a homogeneous electron gas with a density of  $n(r)$  (Wright *et al.*, 2014). It is expressed by the equation;

$$E_{xc}^{LDA}[n(r)] = \epsilon_{xc}^{\text{hom}}(n(r))dr \quad \dots (3.57)$$

Where;

$\epsilon_{xc}^{\text{hom}}$  = function of the electron density  $n(r)$ .

LDA has demonstrated its efficacy in accurately predicting elastic modulus, vibrational frequencies as well as phase stability across a range of systems. However, the model

inaccurately predicts the properties related to magnetism of large-scale compounds and greatly underestimates the magnitude of the bandgap (Manyali *et al.*, 2014). For systems with slowly fluctuating charge densities, the LDA is frequently surprisingly precise and typically produces excellent results. Since the LDA tends to prefer more homogenous systems and over binds molecules and solids, its shortcomings are already well known. These inaccuracies are accentuated and the bond lengths are excessively short in weakly bonded systems. Geometries provide favorable properties, with bond lengths and angles demonstrating a high level of precision, typically within a narrow range of deviation, in systems where the Local Density Approximation exhibits satisfactory performance. The estimated estimates for quantities like the dielectric and piezoelectric constants are 10% higher than the experimental values. Despite its simplicity, LDA works reasonably well in systems where the charge density is slowly varying. However it tends to under predict atomic ground state energies and ionization energies, while over predicting binding energies. It is also known to overly favour high spin state structure.

Several experimentally important physical parameters may be estimated to a relevant degree of accuracy, making DFT-LDA preferable to techniques like Hartree-Fock. In cases in which it is not apparent whether or not the LDA applies, complications may arise.

### **3.8.5 Generalized Gradient Approximation (GGA)**

The expansion of the density matrix in terms of its derivatives and density, known as the semi-classical expansion, can be seen as an initial approximation to the local density approximation. It incorporates the consideration of charge density gradients. The subsequent equation illustrates the potential expression of the exchange-correlation-energy which can be illustrated by the equation;

$$E_{xc1}^{GGA}[n(r)] = \int \epsilon_{xc}(n(r), \nabla n(r)) dr \quad \dots (3.58)$$

The description of binding energies of real systems using the Local Density Approximation was significantly improved with the application of the Generalized Gradient Approximation. However it performs a poor job of precisely treating the hydrogen bond and predicting the lattice parameters. Although GGA seems superior to LDA, it too has a number of drawbacks. GGA fails to accurately treat the hydrogen's bond which is clearly manifested through expansion and hence softening of bonds.

### 3.8.6 Hybrid Functional

Hartree-Fock approaches overestimate the band-gap, whereas LDA and GGA both undervalue it in computations. To overcome the above threat, hybrid functional has been developed; however, their high computational cost presents a problem. A fractional Hartree-Fock exact exchange energy and an explicit density functional are combined to create hybrid functional. The goal of this combination is to accurately forecast band gaps and total energies given as;

$$E_{xc} = \int_0^1 U_{xc}^{\xi} d\xi \quad \dots (3.59)$$

Where;

$U_{xc}$  = the exchange correction energy

$\xi$  = interelectronic coupling strength parameter.

### 3.8.7 The Perdew, Burke, Ernzerhof Exchange Correlation Functional

When employed for the calculation of atomic positions, it overestimate the length of the bonds, resulting in an average error and absolute mean error of approximately 0.01 (Perdew *et al.*, 1998). Consequently, its utility is substantially diminished compared to LDA, which produces a mean error of 0.001. In order to determine bond energies, the

PBE method is frequently utilized due to its proven ability to significantly reduce the average absolute error to a level approaching chemical precision. Because of its construction, which guarantees that both the correlation and exchange components maintain a number of physical features, it was selected for this study. In addition, it works well with the closed system that this article is exploring.

### 3.9 Plane Waves

The study of the interactions between nucleus and electrons was addressed by employing the Density Functional Theory and the Born-Oppenheimer approximation. This approach facilitated the formulation of the single particle problem, which pertains to a system consisting of 60 stationary nuclei that move within an effective potential. The expansion of plane waves in the Kohn-Sham wave function plays a significant role in the computation of the total energy of periodic solids. The solutions to the Schrödinger equation for a single particle, characterized by a periodic potential and exhibiting periodicity, can be described using Bloch's theorem given by;

$$\varphi_{kj}(r) = e^{ikr} u_{kj}(r) \quad \dots (3. 60)$$

The electronic states are categorized using the same  $k$  vector, which is determined within the initial Brillouin zone. The given segment may be expanded by employing a basis set comprised of plane waves, exhibiting the characteristic periodicity observed in a crystal structure.

$$u_{kj}(r) = \sum_G C_{jG} + ke^{i(k+G)r} \quad \dots (3. 61)$$

Where;

$$\mu_{kj}(r) = \sum_G C_{jk} + Ge^{ikr} \mu_{kj}(r) \quad \dots (3. 62)$$

Kohn-Sham equations are given as;

$$\left[ -\frac{\hbar^2}{2m} \nabla^2 + V_{eff}(r) \right] \varphi_{kj}(r) = \epsilon_{kj}(r) \quad \dots (3.63)$$

Where;

$$V_{eff}(r) = V_{ext}(r) + V_H(r) + V_{xc}(r) \quad \dots (3.64)$$

And

$$n(r) = 2 \frac{\Omega_c}{2\pi^3} \sum_j \int |\Psi_{kj}(r)|^2 \Theta(E_F - C_{kj}) d^3k \quad \dots (3.65)$$

Where,  $V_{ext}, V_H, V_{xc}$  respectively, stand for the nuclei's exterior, Hartree, and exchange correlation potentials. The expression's factor 2 accounts for the spin  $\uparrow$  and  $\downarrow$ , and  $\Theta$  is a step function that can either be 0 or 1. The Fermi energy is determined using the quantity of electrons,  $N_e$ , present within the single cell. It represents the energy level with the maximum energy that is occupied by a single particle. This energy level is represented as;

$$\int_{\Omega_c} n(r) d^3r \quad \dots (3.66)$$

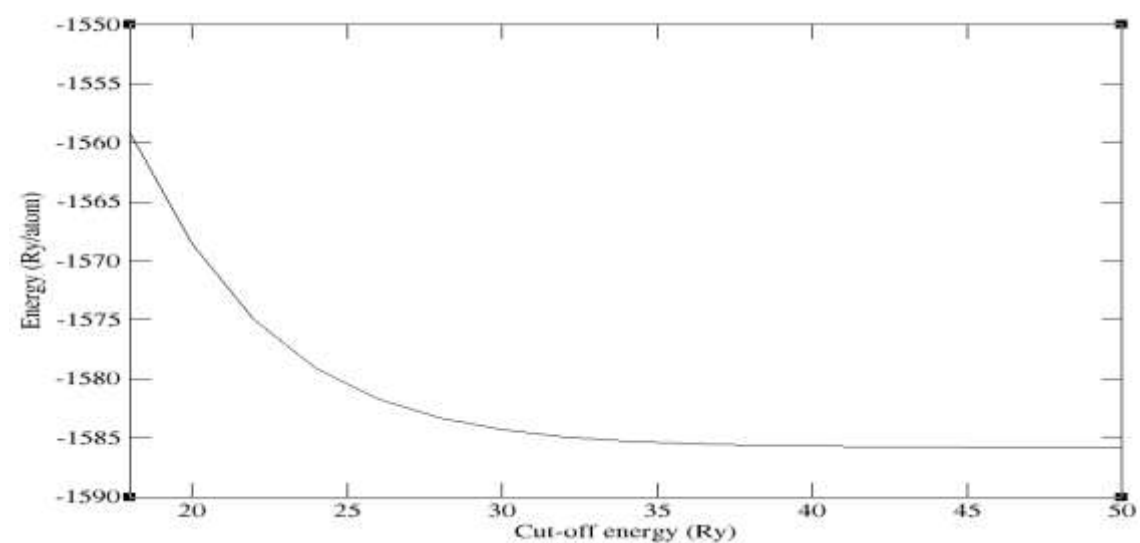
Bloch's theorem facilitates the extension of electronic wave functions at every K-point through the utilization of a discrete set of plane waves. This theorem has been employed to address the problem of computing an infinite quantity of electronic states at an unlimited quantity of K-places distributed within a single unit cell. The current method still necessitates an infinite quantity of computations for the various K-points, therefore resulting in only a marginal improvement. The wave functions at a specific point can be represented by a wave function that occurs on a single k-point in k-space due to the similarity of electronic states at neighboring k-points (Yang & Whitfield, 2023).

### 3.10 Energy Cut-off

In the analysis of a material, the Plane Wave Basis Energy is computed using DFT. The investigation of cut-off energy optimization was conducted using a constant k-point-mesh. The energy cut-off convergence for  $\text{AlCCr}_3$  is depicted in Figure 3.

**Figure 3**

*Total Energy Convergences with Plane Wave Cut-Off*



The convergence test for the k-point grid as well as plane-wave energy cut-off was conducted at certain lattice constants, and the atomic positions were relaxed at a temperature of 0 Kelvin. It was important to adjust the volume while relaxing the atomic coordinates in every DFT computation. The choice of a k-point grid for which the results are anticipated to converge, followed by the system being simulated using Quantum Espresso by gradually increasing values of Energy Cut off. The Energy Cut-off values derived and their output Rydberg's energy values were displayed as shown in Figure 3 above. The figure shows that an energy cut-off of less than 30 Ry is insufficient; hence values higher than 30 Ry should be used. However, larger energy cut-off does not improve accuracy; instead, it lengthens CPU time, raising the cost of calculation.

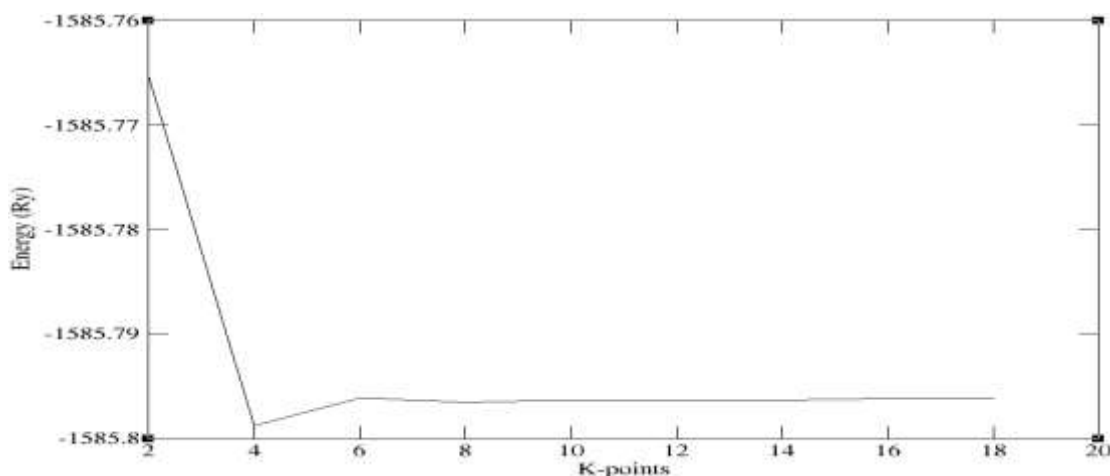
### 3.11 K-Points

Electronic states are only allowed at specific k-points that are determined by the boundary limitations imposed on the bulk solid. The quantity of permissible k-points exhibits a direct relationship with the volume of the solid. However, it should be noted that at each of the infinitely many k-points that constitute the solid's infinite number of electrons. The Bloch theorem is employed to account for periodicity and replaces the computation of an infinite set of electronic wave functions with the computation of a finite set of electronic wave functions at an infinite number of k-points. The determination of the electronic potential in a bulk solid relies on the occupied states. In theory, an endless number of calculations would be required to accurately compute this potential. K-points in close proximity have nearly indistinguishable electronic wave functions. The electronic wave functions can be expressed across a specific region of k-space by utilizing the wave functions at a solitary k-point. In this scenario, the determination of the electronic potential and, consequently, the overall energy of the solid can be achieved by employing a restricted set of electronic states (k points). The generation of atypical k-points was automated in this work by the utilization of the Monkhorst-Pack method. The Monk Horst-Pack approach involves integrating the irreducible portion of the Brillouin Zone. Due to the recognized requirement of transition metals for extensive k-point grids, a comprehensive optimization technique was employed. The K-point size for  $\text{AlCCr}_3$  upon convergence is depicted in figure 4. Higher *K-points* are recommended but do not really boost accuracy



**Figure 4**

*Energy vs. K-Points Graph*



### **3.12 Pseudopotential Approximation**

Pseudopotentials ( $V^{Ps}$ ) are used to improve computational efficiency by substituting an effective potential at the center of an atom. It is generally agreed that an atom chemical as well as physical properties are entirely dictated by their valence electrons. This leads to the development of the pseudo potential approximation. This technique takes for granted that the core electrons are immobile and that ionic interactions are entirely charged. The pseudopotential approximations leverage this trait in order to avoid incorporating the atom's center states. Instead of the formidable strong nuclear potential, the pseudopotential is employed to impose a reduced "pseudo-potential" on a series of pseudo-wave functions apart from other authentic valence wave functions. In order to get the major significant of the outermost electrons in the electronic structural problem, a pseudopotential approximation is a fantastic tool.

The electrons located in the inner regions of an atom often exhibit strong binding to the nucleus, rendering them relatively resistant to external perturbations. This resilience can be attributed to the smooth nature of their wave functions when positioned farther out from the nucleus. However, as these electrons get closer to the nucleus, their wave

functions experience fast fluctuations. Determining the valence of an atom is mostly the job of the wave functions on the periphery of the nucleus. Since the electronic density of the core and cancels itself, it is assumed that the core is at rest even if it serves as a border restriction on the wave functions beyond its region. The authentic Columbic potential is more robust and refined than any imitation. Pseudopotentials with comparable behavior to all electron potentials are selected instead. These pseudopotentials loosen the norm conservation requirement somewhat, but still need the scattering properties to match throughout a broader energy range. The purpose of incorporating the charge augmentation mechanism in the pseudopotentials is to reinstate the principle of norm-conservation, hence ensuring the appropriate allocation of valence charges within the center region. Besides contributing to improved smoothness and transferability, they permit the former.

### **3.12.1 Norm conserving pseudopotential**

The aforementioned statements serve to streamline the understanding of core electrons by immediately focusing on their properties and properties. A norm-preserving pseudopotential is employed to ensure the normalization of the motion of the non-periodic core electrons. The introduction of periodicity in the motion of electrons enables the attainment of a Gaussian distribution through the process of normalizing. This probability distribution facilitates faster convergence. In the context of forces and stresses, even little alterations in either magnitude or direction have the potential to induce disruptions within the system.

### **3.12.2 Ultra Soft Pseudo-Potential**

Practical solutions to the self-consistent Kohn-Sham equation necessitate the utilization of many approximations hence several techniques have been devised to achieve quick convergence at low cost to accuracy (Pickett, 1989). The utilization of pseudo-potentials

incorporating ion cores, which encompass deep inner core electrons and nuclei, enables the effective utilization of plane wave basis sets on electronic structure calculations. This is achieved even though ions have a limited impact on the properties of solids. Hellmann first proposed the use of pseudo-potentials in 1936; they substitute an effective potential term for the Coulomb potential in the Schrodinger equation (Hellmann & Kassatotschkin, 1936). This is due to the fact that pseudo-potentials imitate the properties of ion cores (Kresse & Joubert, 1999).

Pseudo-potential approaches have common theoretical underpinnings, but different methods are used in their production, resulting in a variety of distinct forms. Most plane-wave electronic structure codes use either a norm-conserving or ultra-soft pseudo-potential. They make it possible to properly numerically converge with acceptable computer resources by using a basis set having substantially low cut-off to represent the electron wave-function (H.-Y. Lee et al., 2012). Bloch proposed the projector augmented wave pseudo-potential in 1994 as a means of transforming a standard Kohn-Sham problem with numerically inconvenient behavior with some other variables built in (Blöchl, 1994).

The chosen method effectively captures the nodal properties of the wave function of valence electrons and also enables the incorporation of higher core states inside the spin coupling interaction mechanism (Wang & Perdew, 1991). DFT computations may be performed with improved computer efficiency using this technique, which is an extension of the pseudopotential as well as linear augmented-plane-wave approaches. In comparison to ultra-soft pseudo-potentials, PAW potentials tend to be more precise (Kresse & Joubert, 1999). The core radii of the projector augmented wave potentials are comparatively lower than those of the ultra-soft pseudo potential (Vosko *et al.*, 1980). The basis sets as well as energy cut-off required are comparatively greater as a result of

the decreased core radii of the projector augmented wave potentials. If such pinpoint accuracy is unnecessary, the more primitive may be utilized instead. The computational cost of model structures incorporating any of these aspects does not exhibit a higher expense when employing the projector augmented wave method compared to the ultrasoftpseudopotential approach, despite the larger size of the basis set (Kresse & Joubert, 1999). This phenomenon can be attributed to the negligible alterations in the energy cut-offs for carbon, nitrogen, and oxygen. The inner core electrons and nuclei were modeled using ultrasoft pseudo-potentials in this investigation. Ultra-soft pseudopotentials converge more quickly than norm-conserving ones.

### 3.13 Self-consistent Field (scf) Cycle

In computational techniques, the Schrodinger equation is expressed as;

$$H\psi_i(r) = \left[ -\frac{1}{2}\nabla^2 + V_{eff} \right] \psi_i(r) = \varepsilon_i \psi_i(r) \quad \dots (3. 67)$$

The  $V_{eff}$  is expressed as;

$$V_{eff}(r) = V_{ion}(r) + V_H[n(r)] + V_{xc}[n(r)] \quad \dots (3. 68)$$

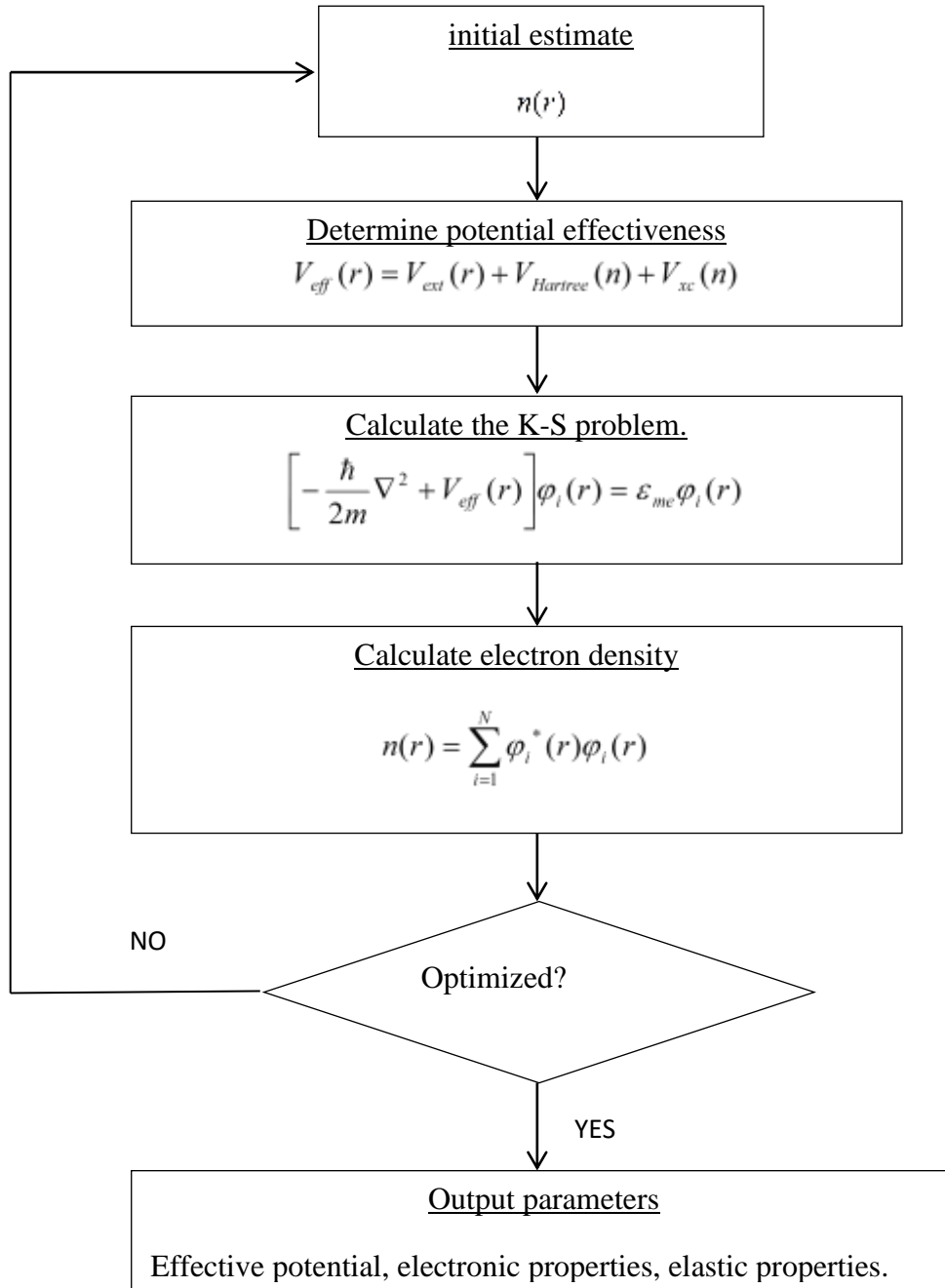
The Hamiltonian operator, denoted as H, encompasses the operator for kinetic energy as well as an effective potential based on the equation;  $e = me = 1$ . The electron density  $n(r)$  is calculated using the wave function,  $H\psi_i(r)$ , hence it follows that relies on itself. A stepwise solution to the Kohn-Sham equation is obtained by initially approximating the electron density, followed iteratively updating it up to a point where input and output electron densities,  $n(r)$  as well as  $n'(r)$ , respectively, become nearly equal within a specified threshold. The iteration process is halted once this condition is met. The self-consistent field method, depicted in Figure 5 as a flowchart, illustrates this concept. The flowchart illustrates the sequential procedures involved in solving the Kohn-Sham equations pertaining to a certain collection of the nuclear centers. The construction of the

periodic table involves initially formulating informed hypotheses on the wave function of hypothetical atoms possessing atomic numbers ( $Z$ ) and masses ( $A$ ) that align with the observable properties of real atoms.

The determination of charge density is achieved by establishing the  $ecutrho$ , a value contingent upon the specific pseudopotential employed. The formation of a solid is achieved through the determination of the atomic locations within the unit cell, the Bravais lattice structure, the nature of element present, and the lattice constant. In order to address the issue arising from the coulombic potential exerted by the nucleus on the electrons, the implementation of pseudo potentials is deemed necessary. The selection of a specific pseudo potential dictates the corresponding exchange-correlation solution that needs to be identified. The equations of Kohn-Sham pertaining to a single particle were resolved by executing a computer script that utilizes an executable command to determine the Hamiltonian and potential, thereby yielding a novel electron density. The procedure is repeated until targeted energy level is attained. Upon achieving convergence, the system's energy level undergoes a reduction to its minimum value, while the interatomic forces approach a state of minimal magnitude. The attainment of this outcome was facilitated by establishing the convergence threshold at a magnitude ranging from  $10^{-12}$  Ry. It is not necessary to have an exact solution to the relevant eigenvalue problem at the beginning of the *scf* cycle if it would delay the procedure's convergence and the K-S equations must be solved repeatedly. When the *scf* method has almost converged, the effective potential  $V_{eff}$  scarcely fluctuates; hence there are less and fewer shifts in the eigenvalue.

**Figure 5**

*Computational schematic representation of the S-C loop for the solution of the K-S Equation*



It is predicted that there is a minimum-energy-providing electronic charge density. Based on these calculations, the effective potential is calculated,  $V_H(r)$ ,  $V_{xc}(r)$  and  $V_{nuc}(r)$ . As a result, Hamiltonian of the system is expressed as;

$$H\Psi_i(r) = \left[ \frac{-1}{2} \nabla^2 + V_{eff} \right] \Psi_i(r) = \varepsilon_i \Psi_i(r) \quad \dots (3. 69)$$

The exact position for the minimum energy is denoted as  $\varepsilon_i$ . Upon normalization the equation becomes;

$$\langle \psi | H | \psi \rangle = E_o \langle \psi | \psi \rangle \quad \dots (3. 70)$$

But;

$$\langle \psi | \psi \rangle = 0 \quad \dots (3. 71)$$

Therefore,  $E_o$  is obtained from the estimated charge density,  $n(r)$

Consequently;

$$n(r) \propto E_o \quad \dots (3. 72)$$

This illustrates self-consistency by showing that the calculated density is the same as the expected density. If there is a discrepancy between the calculated density and the predicted density, the process is repeated until the two values agree. Using the charge density from the prior step, a new estimate for the density is generated. The selection of the basis set entails making an important distinction between the starting data and the solution or parameter optimization. The choice of the advanced crystal grid and atomic orbital calculation is made during this step. The Schrödinger equation must then be resolved as a following step. Since there can only be one electron system in an atom, this is accomplished by calculating the density of single electron wave functions. As an example, the geometrical properties of a crystal grid and the energy connection between its locations may be calculated using the findings (Kravtsova *et al.*, 2009). The findings of parameter calculations for atomic structures may be utilized to estimate the material's strength (Iskandarov *et al.*, 2011). The findings of parameter calculations may also be utilized to ascertain the properties of the electron structure, the band structure, and the elastic properties (Alemany, 2013).

## CHAPTER FOUR

### RESULTS AND DISCUSSIONS

#### 4.1 Introduction

This chapter presents the findings interpretation and discussion of the electronic structure properties, elastic, superconducting as well as thermodynamic properties of hexagonal antiperovskite  $XCCr_3$  ( $X=Al, Ga$  or  $Zn$ ) and also compares the results with other studies.

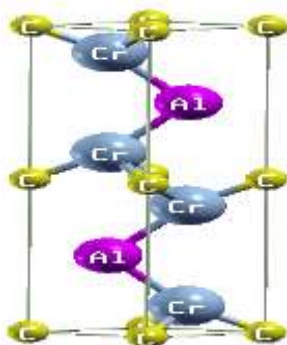
#### 4.2 Electronic Structural Properties of Hexagonal Antiperovskite

##### 4.2.1 Structural Properties

Hexagonal phase of chromium based antiperovskite with space group  $P6_3/mmc$  was considered. The original structure from the Aflow database and the optimized structure were simulated using the same values for  $ecutwfc$  and  $ecutrho$  using Xcrysden software (Kokalj, 1999). In the *ab-initio* calculations, the first step is determined by the equilibrium parameters of the structural properties. The lattice parameter of the compound was obtained by computing of full energy for the unit cell versus the volume. The structures were visualized before and after optimization. The optimization of the volume was achieved by minimizing the overall energy with regard to the volume, employing Murnaghan's equation of state.

**Figure 6**

*Crystal Structure of Unit Cell of  $AlCCr_3$*



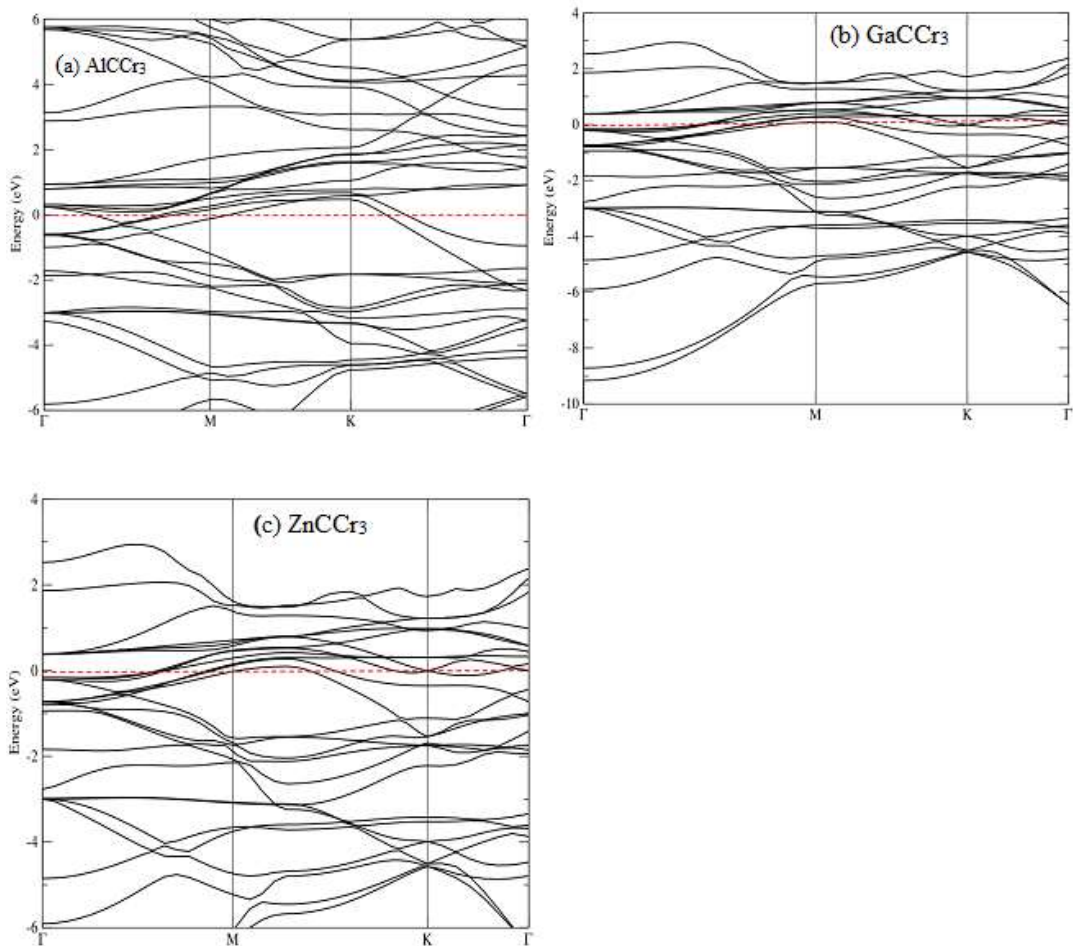


### 4.2.2 Electronic Properties

Figure 7 depicts the predicted band structure of  $XCCr_3$  ( $X= Al, Ga$  or  $Zn$ ) in the BZ at ambient pressure with  $FM$  spin configuration along the high symmetry direction. A visible representation of the Fermi level designated by a red line and set at zero can be observed. The band structures of all the three compounds exhibit metallic structures. The bands, which range in energy from  $-6$  eV to  $6$  eV, are mostly made up of the  $Cr-3d$  and  $C-2s$  states, suggesting that the electrons are itinerant.

**Figure 7**

*Band structures of (a)  $AlCCr_3$ , (b)  $GaCCr_3$  and (c)  $ZnCCr_3$ .*

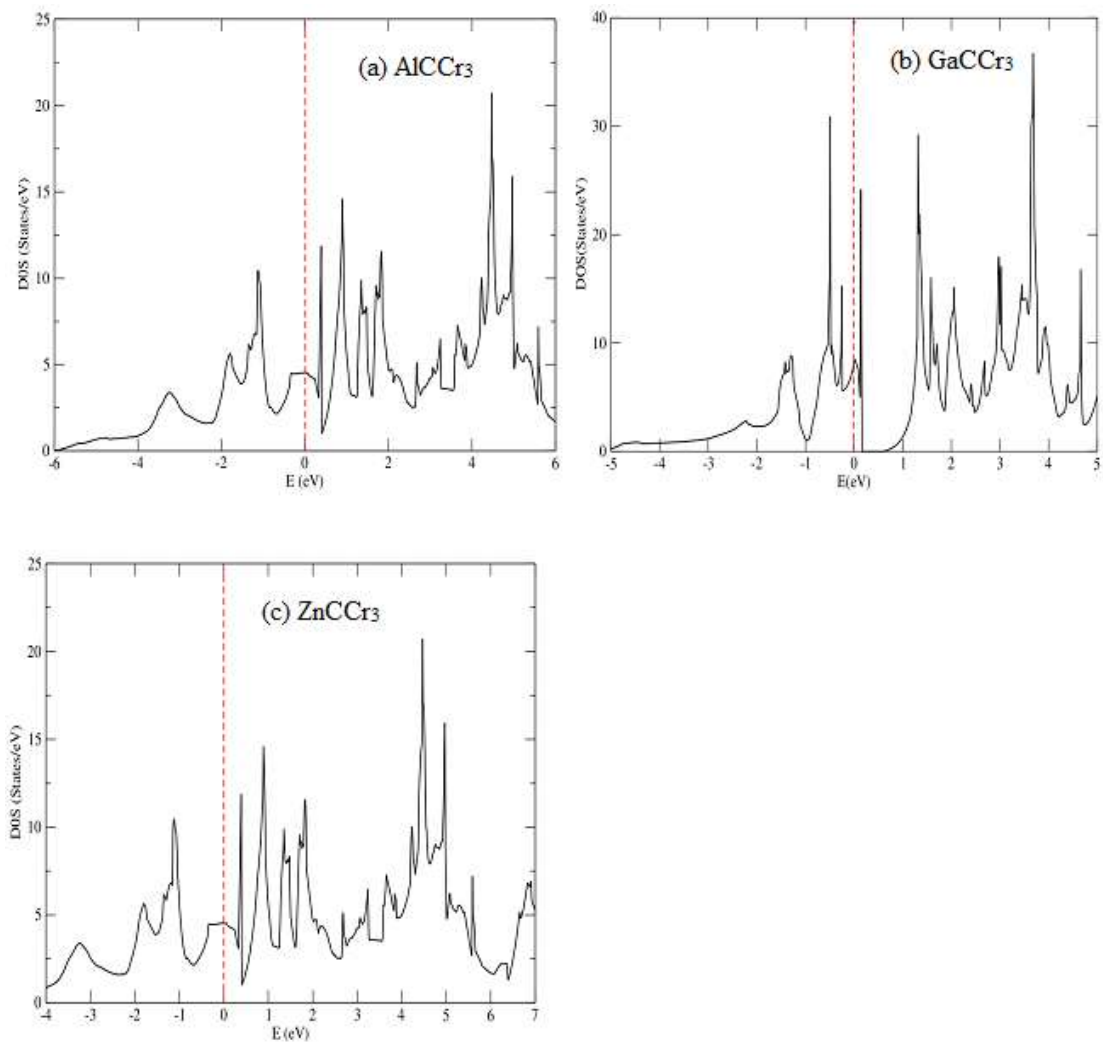


### 4.2.3 Density of States

It was estimated in order to gain a deeper understanding of the electronic band structure, as depicted in Figure 8 for  $XCCr_3$  ( $X= Al, Ga$  or  $Zn$ ). A significant density of states is seen at the Fermi level, denoted as  $N(E_F)$ , with respective values of 4.89, 5.72, and 4.32 states per electronvolt (states/eV) for  $AlCCr_3$ ,  $GaCCr_3$ , and  $ZnCCr_3$ . This is due to the Fermi level's proximity to the DOS peak.

**Figure 8**

*Densities of the states of (a)  $AlCCr_3$ , (b)  $GaCCr_3$  and (c)  $ZnCCr_3$*



### 4.3 Elastic properties

The correct structural relaxation of the material to the structure's almost zero stress condition was used to calculate the elastic constants tabulated in table 1. The lattice vectors are then subjected to perturbations and the resultant stress tensor is determined, enabling the ionic degrees of freedom to relax. The estimated elastic constant values meet the Born criteria condition and this serves as evidence that the three structures examined in this study exhibit elastic stability.

The lattice parameter of the compound was obtained by computing of full energy for the unit cell versus the volume. The values of total energy were fitted to the Murnaghan's equation of state (Ledbetter, 1977). The lattice constants  $a$  were obtained as; 3.201Å for AlCCr<sub>3</sub>, 3.241Å for GaCCr<sub>3</sub> and 3.20 Å for ZnCCr<sub>3</sub>, which are very near to the experimental values of 3.02, 3.037 and 3.102Å respectively as tabulated in table 1. Considering that the zero-point motion and thermal effects are not taken into account, the calculated lattice constants agree quite well with other studies (Liu et al., 2017). This is largely sufficient to allow the further study of dynamical and thermodynamic properties.

**Table 1**

*Calculated lattice constants in (Å) and elastic constants in GPa*

Material	$a$ (Å)	$C_{11}$	$C_{12}$	$C_{13}$	$C_{33}$	$C_{44}$
AlCCr <sub>3</sub>	5.207	243.2918	28.0521	21.5749	191.9535	116.5725
GaCCr <sub>3</sub>	5.813	189.8909	27.7094	28.8399	178.0325	64.2360
ZnCCr <sub>3</sub>	5.721	187.4470	21.6480	10.6917	105.5867	74.6348

#### 4.3.1 Elastic Anisotropy

When a material exhibit different values when measurements are made along different axes, the material is said to be anisotropic. The response of the elastic properties of solids

to the direction of strain is defined by the elastic anisotropy, denoted by the symbol  $A$ . Table 2 presents the calculated shear-type anisotropy ratios derived using the  $C_{ij}$  measurements.

**Table 2**

*Shear type anisotropic ratios compared to results from other studies*

Material	$A_1$	$A_2$	$A_3$
AlCCr <sub>3</sub> (This work)	0.813	1.083	0.880
(Shao et al., 2014)	0.910	0.981	0.719
GaCCr <sub>3</sub> (This work)	1.189	0.792	0.941
(Shao et al., 2014)	0.780	0.653	0.874
ZnCCr <sub>3</sub> (This work)	0.843	0.900	0.758
(Shao et al., 2014)	0.785	0.874	0.862

The crystal exhibits isotropy when the value of the elastic anisotropy ratio, denoted as  $A$ , is equal to 1. Alternatively, anisotropy can be represented by values of  $A$  which are either smaller or greater than one. All the materials being examined exhibit elastic anisotropy. The results of the computations utilizing the Voigt and Reuss approximations are tabulated in table 3. The obtained values are a little different from the theoretical values by shao *et al.* This may be due to the fact that, the results were compared with hexagonal structure studied in this research, while shao *et al.* studied cubic structure. Furthermore, there was no data on hexagonal structure to compare with at the time of reporting this work.

Substance's ability to endure changes in volume when crushed from all sides is determined by its bulk modulus which directly relates to its ability to withstand change of shape. From table 3, it is noted that ZnCCr<sub>3</sub> has the lowest bulk modulus value and

$\text{GaCCr}_3$  has the greatest value hence it has the highest ability to resist fracture among the three materials examined in this study.

Shear modulus is a number that represents a material's capacity to withstand transverse deformation. A higher shear modulus number implies that the solid is extremely stiff and may need more effort to be bent.  $\text{AlCCr}_3$  has the highest shear modulus value of the three investigated compounds, making it the most capable of resisting plastic deformation.

The tensile elasticity of a material can be measured using a ratio known as the Young's modulus. This refers to the quantification of a material's ability to resist changes in size when subjected to compression or strain along its longitudinal axis. It is calculated by dividing longitudinal stress by strain, and it provides information on a material's stiffness.

The Pugh's ratio gauges a material's ductility or brittleness. This ratio's critical value is listed as 0.5. Brittleness is represented by a number less than 0.5, and ductility is represented by a value greater than 0.5 Table 3's findings demonstrate that all three of the materials' Pugh's ratios are higher than the critical level. This suggests that they are all ductile, even though  $\text{AlCCr}_3$  has the greatest ductility. By dividing the lateral strain by the longitudinal strain in the direction of the stretching force, one may determine Poisson's ratio. The ratio typically ranges from 0 to 0.5. Although  $\text{GaCCr}_3$  has a greater Poisson's ratio than the other two materials, it was found that all three are brittle.

**Table 3**

*A comparative analysis of the results related to Young Modulus,  $E$  in Gpa, Poisson ratio  $\sigma$ , and Pugh Ratio ( $G_H/B_H$ ), alongside the Bulk Modulus and Shear Modulus in Gpa, employing the Voigt, Reuss, and Hill Averaging Scheme.*

Material	$B_V$	$B_R$	$B_H$	$G_V$	$G_R$	$G_H$	$E$	$\sigma$	$G_H/B_H$
AlCCr <sub>3</sub> (This work)	59.57	58.91	59.24	123.75	122.70	123.23	218.31	0.11	2.08
(Shao <i>et al.</i> , 2014)	34.80	51.20	57.35	70.95	103.42	123.21	199.30	0.40	2.15
GaCCr <sub>3</sub> (This work)	80.96	80.90	80.93	73.41	72.57	72.99	168.35	0.15	0.90
(Shao <i>et al.</i> , 2014)	36.99	45.23	54.58	71.51	68.35	67.26	201.53	0.41	1.23
ZnCCr <sub>3</sub> (This work)	43.82	41.16	42.49	85.66	81.77	83.72	151.60	0.09	1.97
(Shao <i>et al.</i> , 2014)	36.23	56.98	50.51	78.56	75.24	89.27	132.25	0.04	1.72

#### 4.3.2 Debye Temperature

The Debye temperature is a basic parameter that corresponds with a variety of solid-state physical properties, including specific heat, elastic constant and superconducting temperature. The Debye temperatures for AlCCr<sub>3</sub>, GaCCr<sub>3</sub>, and ZnCCr<sub>3</sub> are 718.557K, 483.170K, and 509.329K, respectively, as tabulated in table 4. AlCCr<sub>3</sub> exhibits the greatest Debye temperature among the considered materials, hence indicating superior interatomic bonding, melting point, hardness, and conductivity to heat relative to the rest of the materials.

**Table 4**

*A comparison between the values obtained by the use of the Voigt-Reuss-Hill Average method for Compressional ( $V_P$ ), Bulk ( $V_B$ ), Shear ( $V_G$ ), Average Debye Sound Velocities ( $V_D$ ), Solid Density  $\rho$ (g/cm<sup>3</sup>), and Debye Temperature  $\Theta_D$  (K), and the corresponding values reported in earlier studies.*

Material	$V_P$	$V_B$	$V_G$	$V_D$	$\rho$ (g/cm <sup>3</sup> )	$\Theta_D$ (K)
AlCCr <sub>3</sub> (This work)	6790.41	3495.72	5041.55	5416.13	5.43	718.56
(Shao <i>et al.</i> , 2014)	-	-	-	-	-	532.43
GaCCr <sub>3</sub> (This work)	5340.79	3598.69	3417.63	3750.01	5.59	483.17
(Shao <i>et al.</i> , 2014)	-	-	-	-	-	497.12
ZnCCr <sub>3</sub> (This work)	5001.94	2626.48	3686.56	3940.87	5.51	509.33
(Shao <i>et al.</i> , 2014)	-	-	-	-	-	524.53

#### 4.4 Superconductivity Properties

The materials had average electron-phonon coupling constant ( $\lambda$ ) that is computed to range between 0.61 and 0.82 (table 5) and less than 1.0, indicating moderate electron phonon coupling strength. This suggests that the average electron-phonon coupling parameter in this material is not significantly influenced by the high frequency phonon modes. The phonon density of states analysis reveals influence of the motions that occur between  $X$  as well as  $Cr$  atoms. This is not unexpected given that  $X$  and  $Cr$  orbitals predominate in the states close to the Fermi energy. Where  $\mu^*$  denotes an effective screening coulomb repulsion parameter and  $\omega_{ln}$  is the logarithmic averaged phonon frequency. The value of  $\mu^*$  is found to be 0.10, giving the values of  $\omega_{ln} = 382.2K$ , 121.64K and 217.56K for AlCCr<sub>3</sub>, GaCCr<sub>3</sub> and ZnNCCr<sub>3</sub> respectively. The value of  $\mu^*$  fluctuates between 0.10 and 0.16 in the majority of research (Dynes, 1972). The superconducting transition temperature is calculated using these values for  $\mu^*$  and  $\omega_{ln}$ .

When the Coulomb repulsion parameter is set at 0.10, the resulting transition temperature values for  $\text{AlCCr}_3$ ,  $\text{GaCCr}_3$ , and  $\text{ZnNCCr}_3$  are 6.82 K, 12.01 K and 8.21 K, respectively. The obtained values for all materials, as presented in table 5, exhibit a high level of agreement with the established experimental results.

**Table 5**

*Density of States (DOS) near the Fermi level and the average electron-phonon coupling parameter ( $\lambda$ ), the logarithmic frequency ( $\omega_{\ln}$ ), and the superconducting transition temperature for the hexagonal  $\text{XCCr}_3$  (A=Al, Ga, or Zn) for this research, as well as a comparison with the results of available previous studies.*

Compound	DOS (states/eV)	$\lambda$	$\omega_{\ln}$ (K)	$T_C$ (K)
$\text{AlCCr}_3$ (This work)	4.89	0.60	382.2	6.82
(Shao <i>et al.</i> , 2014)	3.53	0.61	291.51	6.67
$\text{GaCCr}_3$ (This work)	5.72	0.77	121.64	12.01
(Shao <i>et al.</i> , 2014)	3.08	0.78	253.91	11.29
$\text{ZnNCCr}_3$ (This work)	4.32	0.70	217.56	8.21
(Shao <i>et al.</i> , 2014)	2.81	0.67	260.27	8.23

The link between the vibration frequency  $\omega$  and the wave vector  $q$  is often known as the lattice dynamic theory or as the interlink of dispersion (Gonze *et al.*, 2005). The expression of phonon modes can be described as follows: in a crystal lattice, if an element cell has  $n$  atoms, then there exist a total of  $3n$  modes, consisting of three acoustic modes and twelve optical modes. The phonon spectra as well as the total and partial phonon density of states of the examined antiperovskite material are depicted in Figure 9. The first three phonon modes are low-frequency acoustic modes. The next twelve phonon modes include optical, transversal, and longitudinal modes. Generally, there is



one longitudinal mode and two transversal modes. The fact that all of the frequencies are positive indicates that the structures were dynamically stable.

Gaps were observed at the zone center  $C$  that was divided by optical phonon modes. The observed gaps in between the longitudinal optical ( $LO$ ) and transversal optical ( $TO$ ) phonon modes can be attributed to the discrepancy in mass between atoms  $C$  and  $X$ . The term "splitting" refers to the categorization of this gap as LO-TO and is highlighted using a red line. The splitting observed in this phenomenon can be attributed to the dipole to dipole interactions that arise from the collective electric field resulting from the displacements of ions at the macroscopic level. Because  $X$  atoms have a greater mass than other atoms, it causes the acoustic area (transverse and longitudinal acoustical) to vibrate in accordance with the varied masses of the compound's atoms. The final three phonon modes, on the other hand, are caused by the vibrations of  $C$  atoms, whereas nine optical modes are caused by  $X$  atom vibrations. To the best of our knowledge, no investigation has been done of this property using both theoretical and experimental approaches, as anticipated by our analysis of lattice dynamics.

**Figure 9**

*Phonon frequency curves for (a)  $\text{AlCCr}_3$ , (b)  $\text{GaCCr}_3$  and (c)  $\text{ZnCCr}_3$  along the hexagonal Brillouin zone symmetry lines.*

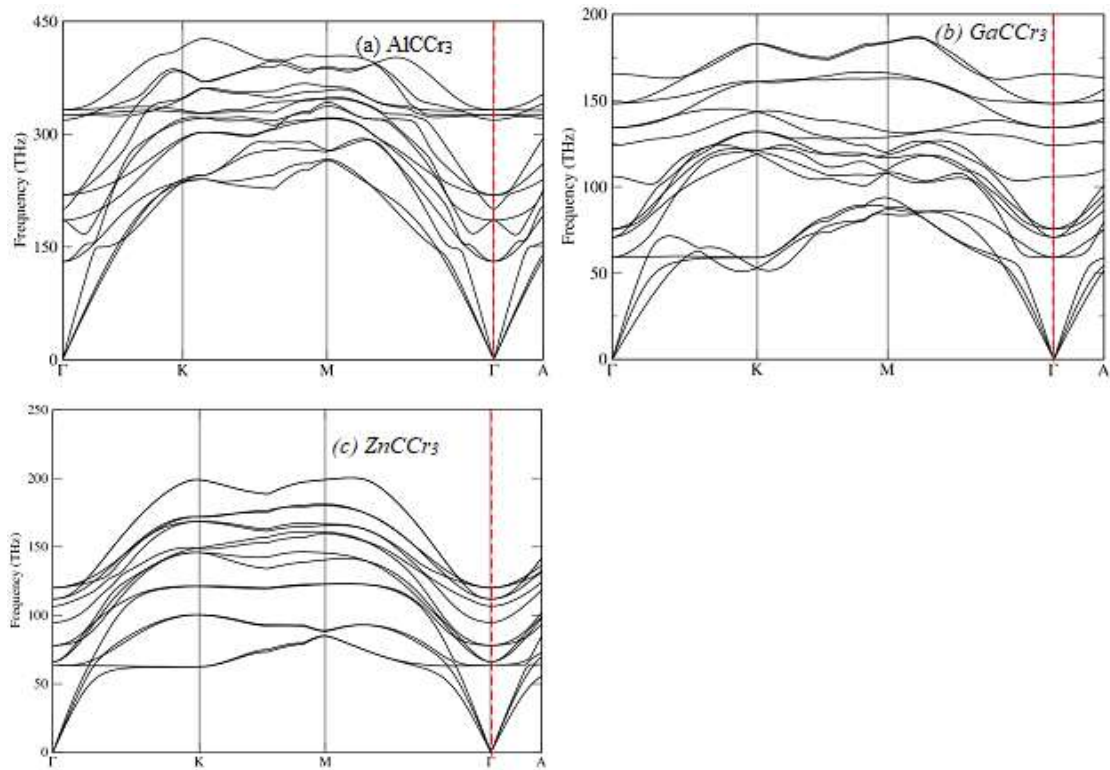
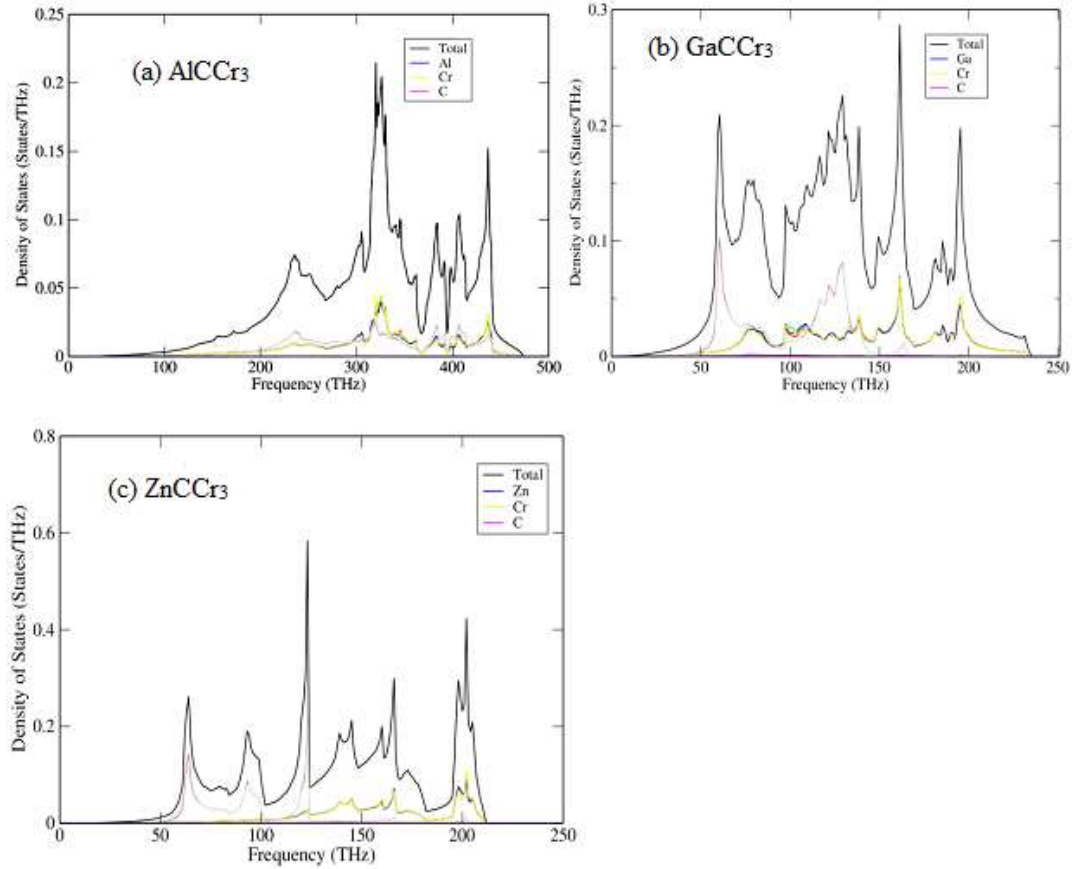


Figure 10 displays the complete and partial phonon density of states pertaining to atoms. The optical modes exhibit two distinct peaks characterized by high frequencies ranging from 180 to 200 THz. These peaks are hypothesized to be associated with vibrational activity originating from the Cr and C atoms. The vibration of the X and Cr atoms causes two peaks to appear at 120 and 280 THz. There is a distinct peak at 180 THz due to the X atoms' low frequency and greater mass vibration.

**Figure 10**

A plot of phonon densities of states of (a)  $\text{AlCCr}_3$ , (b)  $\text{GaCCr}_3$  and (c)  $\text{ZnCCr}_3$ .



#### 4.5 Thermodynamic Properties

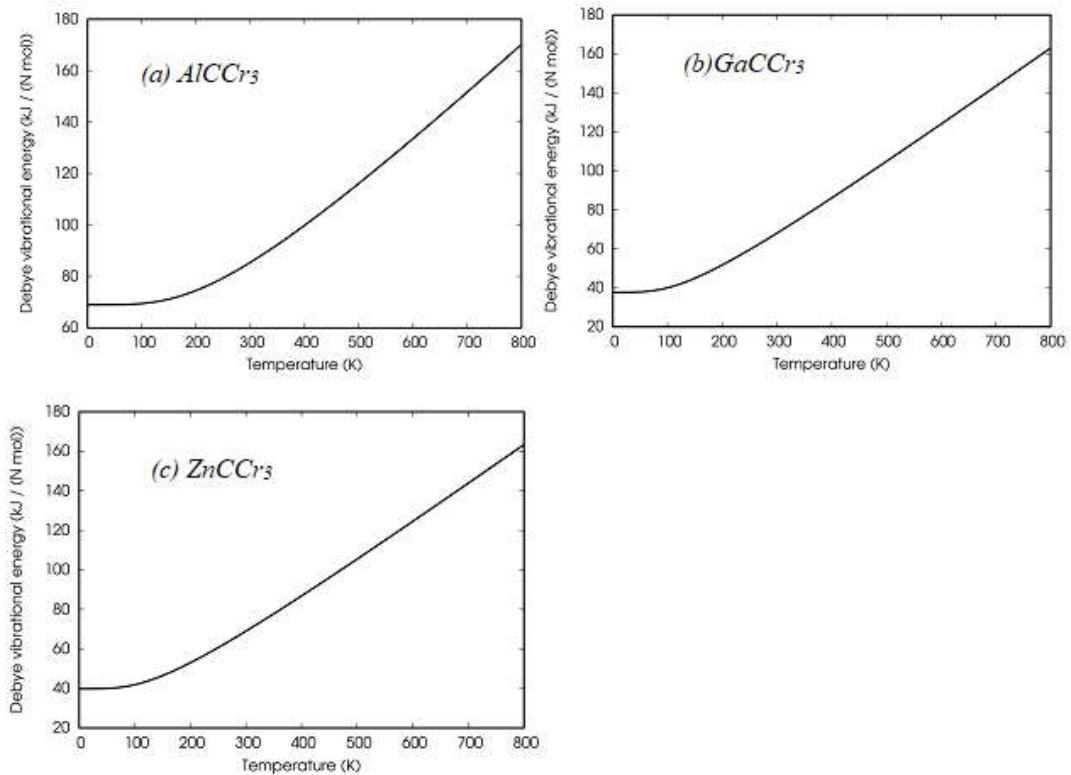
Using the harmonic Debye model, the thermodynamic properties of hexagonal  $\text{XCCr}_3$  ( $\text{X}=\text{Al}$ ,  $\text{Ga}$  or  $\text{Zn}$ ) superconductors were examined. The exchange and correlation terms were also employed in the geometric optimization, which was carried out using ab-initio thermo\_pw code. The temperature range of 0K to 800K is suitable for the use of the quasi harmonic Debye model, which is used to calculate thermodynamic properties of hexagonal structures  $\text{XCCr}_3$  ( $\text{X}=\text{Al}$ ,  $\text{Ga}$ , or  $\text{Zn}$ ). The evaluation of thermodynamic properties under temperature offers critical information on chemical stability, which is required for the identification of these materials in order to utilize them effectively in the industrial sector. The phonon contribution to the Helmholtz free energy  $\Delta F$ , the phonon

contribution to the internal energy  $\Delta E$ , and the constant-volume specific heat  $C_v$ , at temperature  $0-800K$ , are calculated.

The Debye vibrational energy for all the materials remains constant below 100K. Beyond 100K, there are linear increase in vibrational energy with temperature as shown in Figure 11.

**Figure 11**

*Debye energy of vibration (KJ/Nmol) of (a)  $AlCCr_3$ , (b)  $GaCCr_3$  and (c)  $ZnCCr_3$  over different temperatures.*

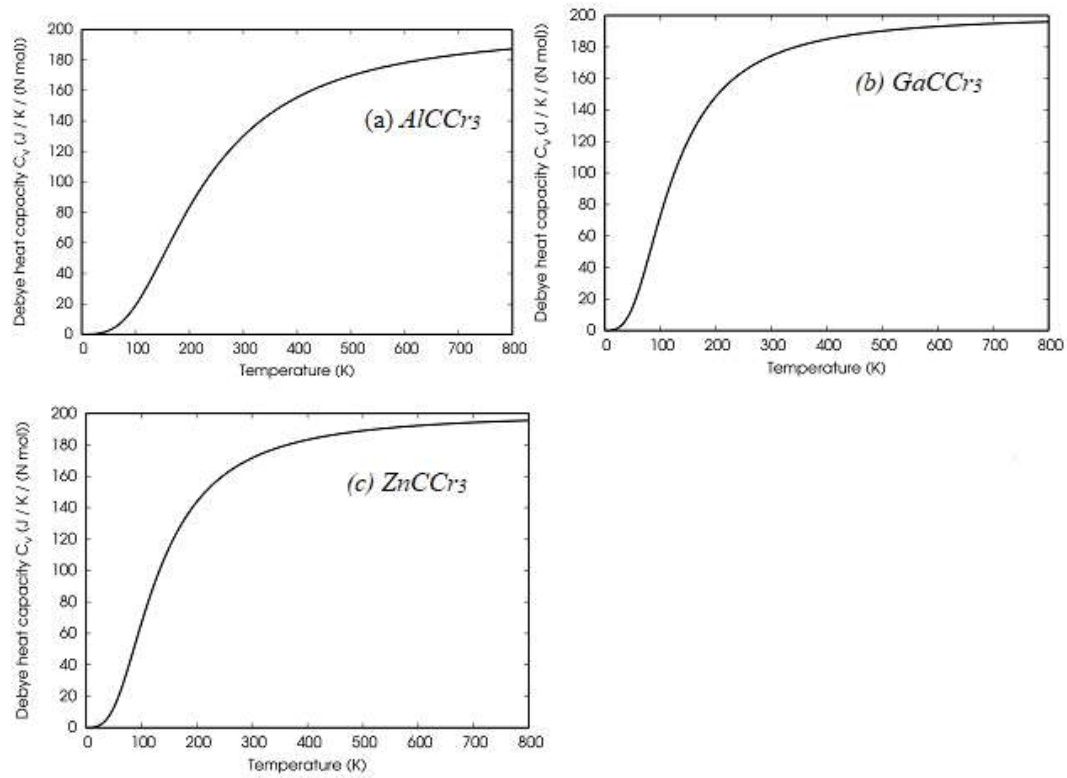


For temperatures below 100K, the values of heat capacity of the compounds are essentially zero. At low temperatures below 200K, the heat capacity of the three compounds obeys the formula  $C = AT^3$  due to anharmonic approximations, which corresponds to the lattice contribution to heat capacity. At high temperatures of 500K and above, the heat capacity  $C_v$  is temperature independent demonstrating that the anharmonic effect on heat capacity is neglected and its value tends to the Dulong-Petit

limit value  $C_V=3NK=190\text{J/K/Nmol}$  for a material with five atoms in the primitive cell as illustrated in Figure 12.

**Figure 12**

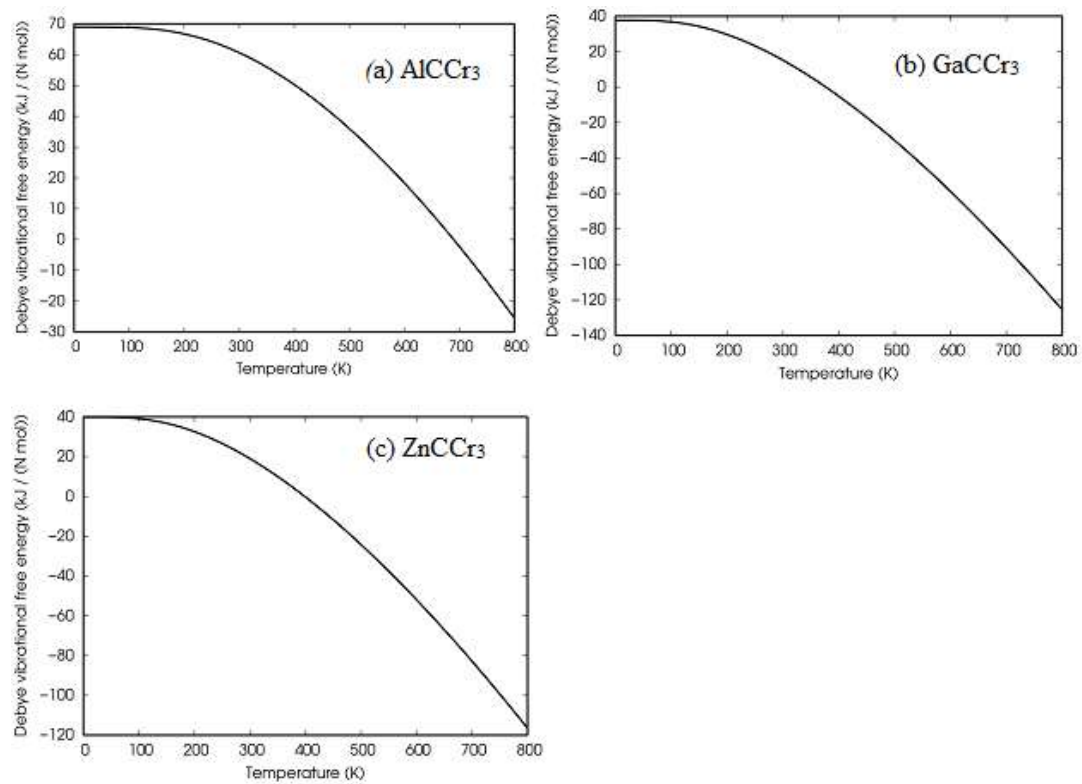
Debye heat capacity  $C_V$  (J/K/(Nmol)) of (a)  $\text{AlCCr}_3$ , (b)  $\text{GaCCr}_3$  and (c)  $\text{ZnCCr}_3$  at various temperatures.



For temperatures beyond 100 K, however, vibrational free energy decreases because entropy increases with temperature as illustrated in Figure 13.

**Figure 13**

*Debye vibrational free energy (J/K/(Nmol)) of (a) AlCCr<sub>3</sub>, (b) GaCCr<sub>3</sub> and (c) ZnCCr<sub>3</sub> at various temperatures.*



## CHAPTER FIVE

### SUMMARY, CONCLUSION AND RECOMMENDATIONS

#### 5.1 Introduction

This chapter provides a detailed summary of the study done with the objective of employing first principles computational modeling using the quantum espresso program, which is based on density functional theory. Conclusion and recommendations on the study of the hexagonal phase  $XCCr_3$  ( $X=Al, Ga, Zn$ ) is presented.

#### 5.2 Summary

##### 5.2.1 Electronic Structure Properties

The primary goal of this work was to investigate the superconducting properties of  $XCCr_3$  ( $X=Al, Ga, \text{ or } Zn$ ) through the analysis of electronic structure, elastic, superconductivity, and thermodynamic properties. The calculated lattice constants were 5.207Å, 5.813Å and 5.721Å for  $AlCCr_3$ ,  $GaCCr_3$  and  $ZnCCr_3$  respectively and are in good agreement with the previous available theoretical work.

##### 5.2.2 Elastic Properties

The obtained results for elastic constant showed that, the materials under study were mechanically stable, as defined by Born stability criterion. The relatively high values of the elastic constants also demonstrated the research materials' excellent resistance to deformation. The three compounds were ductile in nature and had comparable thermal properties, as this study decisively demonstrates. Debye heat capacity, Debye vibrational energy and Debye temperature were all thoroughly investigated using thermo\_Pw code, with the findings tabulated.  $AlCCr_3$  has a substantially higher Debye temperature than  $GaCCr_3$  and  $ZnCCr_3$ , which shows that it is strongly bound, much stiffer and much harder.

### 5.2.3 Superconductivity Properties

DFPT was used to obtain the relation of the dispersion of the studied compound, in which 15 phonon modes were obtained, with three acoustic modes and twelve optical modes. At the center of the Brillouin zone, there are gaps and splitting between the longitudinal and transversal optical modes. All the materials studied had average electron-phonon coupling parameters of between 0.6 and 0.8, which indicates a moderate level of electron phonon coupling strength. The obtained superconducting transition temperatures of 6.82 K, 12.01 K and 8.21 K for  $\text{AlCCr}_3$ ,  $\text{GaCCr}_3$  and  $\text{ZnCCr}_3$  respectively are comparable with other studies.

### 5.2.4 Thermodynamic Properties

Density functional theory and linear response theory were used to determine the thermodynamic properties. The phonon frequencies at the Brillouin zone centre ( $\Gamma$  point), as well as  $X$  and  $L$  points and the phonon dispersion curves with corresponding phonon density of states were obtained. The thermodynamic properties including the phonon contribution to the Helmholtz free energy  $\Delta F$ , the phonon contribution to the internal energy  $\Delta E$ , the entropy  $S$ , and the constant-volume specific heat  $C_V$  were determined within the harmonic approximation based on the calculated phonon density of states.

## 5.3 Conclusion

Engineers may design and create appropriate materials for electrical conductivity with the use of knowledge of electronic structure, elastic constants, superconductivity properties and thermodynamic properties. The findings of this work can be utilized to guide experimentalists in developing high temperature superconductors.



#### **5.4 Recommendations for Further Research**

This research on the properties of  $XCCr_3$  ( $X=Al, Ga, Zn$ ) recommends the following;

- i. This work investigated only hexagonal structure where only five atoms were used and displaced within the cell. Thus, there is need for multi-atom structures to be studied.
- ii. Optical properties of antiperovskites materials are significant properties that could be investigated for more interesting applications.
- iii. Further studies based on pressure induced phase transition will be significant for determination of the superconducting transition temperature of other phases.

## REFERENCES

- Agora, J. O., Otieno, C., Nyawere, P. W. O., & Manyali, G. S. (2022). Elastic behavior, pressure-induced doping and superconducting transition temperature of  $\text{GdBa}_2\text{Cu}_3\text{O}_{7-x}$ . *Journal of Physics Communications*, 6(1), 15004. <https://doi.org/10.1088/2399-6528/ac438c>
- Aleman, P. (2013). Analyzing the electronic structure of molecules using continuous symmetry measures. *International Journal of Quantum Chemistry*, 113(14), 1814–1820. <https://doi.org/10.1002/qua.24373>
- Allen, P. B., & Dynes, R. C. (1975). Transition temperature of strong-coupled superconductors reanalyzed. *Physical Review B*, 12(3), 905–922. <https://doi.org/10.1103/PhysRevB.12.905>
- Amara, K., Zemouli, M., Elkeurti, M., Belfedal, A., & Saadaoui, F. (2013). First-principles study of  $\text{XNMg}_3$  (X=P, As, Sb and Bi) antiperovskite compounds. *Journal of Alloys and Compounds*, 576, 398–403. <https://doi.org/10.1016/j.jallcom.2013.06.003>
- Asano, K., Koyama, K., & Takenaka, K. (2008). Magnetostriction in  $\text{Mn}_3\text{CuN}$ . *Applied Physics Letters*, 92(16). <https://doi.org/10.1063/1.2917472>
- Baerends, E. J., Ellis, D. E., & Ros, P. (1973). Self-consistent molecular Hartree—Fock—Slater calculations I. The computational procedure. *Chemical Physics*, 2(1), 41–51. [https://doi.org/10.1016/0301-0104\(73\)80059-X](https://doi.org/10.1016/0301-0104(73)80059-X)
- Bardeen, J., Cooper, L. N., & Schrieffer, J. R. (1957). Theory of Superconductivity. *Physical Review*, 108(5), 1175–1204. <https://doi.org/10.1103/PhysRev.108.1175>
- Bennemann, K. H., & Garland, J. W. (1973). Theory for superconductivity in Pd-H and Pd-D systems. *Zeitschrift Für Physik*, 260(5), 367–374. <https://doi.org/10.1007/BF01397961>
- Blöchl, P. E. (1994). Projector augmented-wave method. *Physical Review B*, 50(24), 17953–17979. <https://doi.org/10.1103/PhysRevB.50.17953>
- Cederbaum, L. S. (2004). *BORN–OPPENHEIMER APPROXIMATION AND BEYOND* (pp. 3–40). [https://doi.org/10.1142/9789812565464\\_0001](https://doi.org/10.1142/9789812565464_0001)
- Davarpanah, S. M., Ván, P., & Vásárhelyi, B. (2020). Investigation of the relationship between dynamic and static deformation moduli of rocks. *Geomechanics and Geophysics for Geo-Energy and Geo-Resources*, 6(1), 29. <https://doi.org/10.1007/s40948-020-00155-z>
- Delft, D. van. (2012). History and significance of the discovery of superconductivity by Kamerlingh Onnes in 1911. *Physica C: Superconductivity*, 479, 30–35. <https://doi.org/10.1016/j.physc.2012.02.046>
- Diener, G. (1990). E. S. Kryachko, E. V. Ludena. Energy density functional theory of many-electron systems. Kluwer Academic Publishers, Dordrecht 1990, XIII + 850 Seiten, Dfl. 425.00, ISBN 0-7923-0641-4. *Crystal Research and Technology*, 25(10), 1130. <https://doi.org/10.1002/crat.2170251005>

- Dolgov, O. V., Golubov, A. A., Mazin, I. I., & Maksimov, E. G. (2008). Critical temperature and the giant isotope effect in the presence of paramagnons. *Journal of Physics: Condensed Matter*, *20*(43), 434226. <https://doi.org/10.1088/0953-8984/20/43/434226>
- Dynes, R. C. (1972). McMillan's equation and the T<sub>c</sub> of superconductors. *Solid State Communications*, *10*(7), 615–618. [https://doi.org/10.1016/0038-1098\(72\)90603-5](https://doi.org/10.1016/0038-1098(72)90603-5)
- Ennassiri, N., Tahiri, N., El Bounagui, O., Ez-Zahraouy, H., & Benyoussef, A. (2018). Structural, electronic, magnetic, and magnetocaloric properties in metallic antiperovskite compound Mn<sub>3</sub>GaC. *Materials Research Bulletin*, *98*, 335–339. <https://doi.org/10.1016/j.materresbull.2017.10.029>
- Gill, P. M. W., Johnson, B. G., Pople, J. A., & Frisch, M. J. (1992). The performance of the Becke-Lee-Yang-Parr (B-LYP) density functional theory with various basis sets. *Chemical Physics Letters*, *197*(4–5), 499–505. [https://doi.org/10.1016/0009-2614\(92\)85807-M](https://doi.org/10.1016/0009-2614(92)85807-M)
- Gonze, X., Beuken, J.-M., Caracas, R., Detraux, F., Fuchs, M., Rignanese, G.-M., Sindic, L., Verstraete, M., Zerah, G., Jollet, F., Torrent, M., Roy, A., Mikami, M., Ghosez, P., Raty, J.-Y., & Allan, D. C. (2002). First-principles computation of material properties: the ABINIT software project. *Computational Materials Science*, *25*(3), 478–492. [https://doi.org/10.1016/S0927-0256\(02\)00325-7](https://doi.org/10.1016/S0927-0256(02)00325-7)
- Gonze, X., Rignanese, G.-M., & Caracas, R. (2005). First-principle studies of the lattice dynamics of crystals, and related properties. *Zeitschrift Für Kristallographie - Crystalline Materials*, *220*(5–6), 458–472. <https://doi.org/10.1524/zkri.220.5.458.65077>
- Göpel, W., Anderson, J. A., Frankel, D., Jaehnig, M., Phillips, K., Schäfer, J. A., & Rocker, G. (1984). Surface defects of TiO<sub>2</sub>(110): A combined XPS, XAES AND ELS study. *Surface Science*, *139*(2–3), 333–346. [https://doi.org/10.1016/0039-6028\(84\)90054-2](https://doi.org/10.1016/0039-6028(84)90054-2)
- Gordon, R. T., Zhigadlo, N. D., Weyeneth, S., Katrych, S., & Prozorov, R. (2013). Conventional superconductivity and hysteretic Campbell penetration depth in single crystals MgCNi<sub>3</sub>. *Physical Review B*, *87*(9), 094520. <https://doi.org/10.1103/PhysRevB.87.094520>
- Gross, E., & Dreizler, R. M. (1976). Thomas-Fermi potentials for quasimolecular collision processes. *Physics Letters A*, *57*(2), 131–134. [https://doi.org/10.1016/0375-9601\(76\)90188-2](https://doi.org/10.1016/0375-9601(76)90188-2)
- Haddadi, K., Bouhemadou, A., Louail, L., Maabed, S., & Maouche, D. (2009). Structural and elastic properties under pressure effect of the cubic antiperovskite compounds ANCa<sub>3</sub> (A=P, As, Sb, and Bi). *Physics Letters A*, *373*(20), 1777–1781. <https://doi.org/10.1016/j.physleta.2009.03.016>
- He, T., Huang, Q., Ramirez, A. P., Wang, Y., Regan, K. A., Rogado, N., Hayward, M. A., Haas, M. K., Slusky, J. S., Inumara, K., Zandbergen, H. W., Ong, N. P., & Cava, R. J. (2001). Superconductivity in the non-oxide perovskite MgCNi<sub>3</sub>. *Nature*, *411*(6833), 54–56. <https://doi.org/10.1038/35075014>

- Hellmann, H., & Kassatotschkin, W. (1936). Metallic Binding According to the Combined Approximation Procedure. *The Journal of Chemical Physics*, 4(5), 324–325. <https://doi.org/10.1063/1.1749851>
- Hetényi, B., De Angelis, F., Giannozzi, P., & Car, R. (2001). Reconstruction of frozen-core all-electron orbitals from pseudo-orbitals. *The Journal of Chemical Physics*, 115(13), 5791–5795. <https://doi.org/10.1063/1.1398097>
- Hohenberg, P., & Kohn, W. (1964). Inhomogeneous Electron Gas. *Physical Review*, 136(3B), B864–B871. <https://doi.org/10.1103/PhysRev.136.B864>
- Iskandarov, A. M., Dmitriev, S. V., & Umeno, Y. (2011). Temperature effect on ideal shear strength of Al and Cu. *Physical Review B*, 84(22), 224118. <https://doi.org/10.1103/PhysRevB.84.224118>
- Jha, P. K. (2005). Phonon spectra and vibrational mode instability of Mg C Ni 3. *Physical Review B*, 72(21), 214502. <https://doi.org/10.1103/PhysRevB.72.214502>
- Johannes, M. D., & Pickett, W. E. (2004). Electronic structure of ZnCNi 3. *Physical Review B*, 70(6), 060507. <https://doi.org/10.1103/PhysRevB.70.060507>
- Kamihara, Y., Watanabe, T., Hirano, M., & Hosono, H. (2008). Iron-Based Layered Superconductor La[O<sub>1-x</sub>F<sub>x</sub>]FeAs ( $x = 0.05–0.12$ ) with  $T_c = 26$  K. *Journal of the American Chemical Society*, 130(11), 3296–3297. <https://doi.org/10.1021/ja800073m>
- Kohn, W., & Sham, L. J. (1965). Self-Consistent Equations Including Exchange and Correlation Effects. *Physical Review*, 140(4A), A1133–A1138. <https://doi.org/10.1103/PhysRev.140.A1133>
- Kokalj, A. (1999). XCrySDen—a new program for displaying crystalline structures and electron densities. *Journal of Molecular Graphics and Modelling*, 17(3–4), 176–179. [https://doi.org/10.1016/S1093-3263\(99\)00028-5](https://doi.org/10.1016/S1093-3263(99)00028-5)
- Koretsune, T., & Arita, R. (2017). Efficient method to calculate the electron–phonon coupling constant and superconducting transition temperature. *Computer Physics Communications*, 220, 239–242. <https://doi.org/10.1016/j.cpc.2017.07.011>
- Kravtsova, A. N., Mazalova, V. L., Yalovega, G. E., Soldatov, A. V., & Johnston, R. L. (2009). Analysis of the X-ray absorption fine structure near the TiL<sub>2,3</sub> edge in free titanium nanoclusters. *Journal of Surface Investigation. X-Ray, Synchrotron and Neutron Techniques*, 3(1), 38–40. <https://doi.org/10.1134/S1027451009010078>
- Kresse, G., & Joubert, D. (1999). From ultrasoft pseudopotentials to the projector augmented-wave method. *Physical Review B*, 59(3), 1758–1775. <https://doi.org/10.1103/PhysRevB.59.1758>
- Krivovichev, S. V. (2008). Minerals with antiperovskite structure: a review. *Zeitschrift Für Kristallographie - Crystalline Materials*, 223(1–2), 109–113. <https://doi.org/10.1524/zkri.2008.0008>

- Ledbetter, H. M. (1977). Elastic properties of zinc: A compilation and a review. *Journal of Physical and Chemical Reference Data*, 6(4), 1181–1203. <https://doi.org/10.1063/1.555564>
- Lee, H.-S., Jang, D.-J., Lee, H.-G., Lee, S.-I., Choi, S.-M., & Kim, C.-J. (2007). Growth of Single Crystals of MgCNi<sub>3</sub>. *Advanced Materials*, 19(14), 1807–1809. <https://doi.org/10.1002/adma.200602194>
- Lee, H. Y., Clark, S. J., & Robertson, J. (2012). Calculation of point defects in rutile TiO<sub>2</sub> by the screened-exchange hybrid functional. *Physical Review B*, 86(7), 075209. <https://doi.org/10.1103/PhysRevB.86.075209>
- Li, C., Chen, W. G., Wang, F., Li, S. F., Sun, Q., Wang, S., & Jia, Y. (2009). First-principles investigation of mechanical and electronic properties of MNi<sub>3</sub> (M=Zn, Mg, or Cd). *Journal of Applied Physics*, 105(12). <https://doi.org/10.1063/1.3156641>
- Liu, Z., Li, H., Fan, C., & Luo, W. (2017). Necessary and sufficient elastic stability conditions in 21 quasicrystal Laue classes. *European Journal of Mechanics - A/Solids*, 65, 30–39. <https://doi.org/https://doi.org/10.1016/j.euromechsol.2017.02.007>
- Ma, H., Ma, Y., Wang, H., Slebodnick, C., Alatas, A., Urban, J. J., & Tian, Z. (2019). Experimental Phonon Dispersion and Lifetimes of Tetragonal CH<sub>3</sub>NH<sub>3</sub>PbI<sub>3</sub> Perovskite Crystals. *The Journal of Physical Chemistry Letters*, 10(1), 1–6. <https://doi.org/10.1021/acs.jpcclett.8b03419>
- Mackenzie, A. P., & Maeno, Y. (2003). The superconductivity of Sr<sub>2</sub>RuO<sub>4</sub> and the physics of spin-triplet pairing. *Reviews of Modern Physics*, 75(2), 657. <https://doi.org/10.1103/RevModPhys.75.657>
- Manyali, G. S., Warmbier, R., & Quandt, A. (2014). First-principles studies of the structural, electronic and optical properties of dinitrides CN<sub>2</sub>, SiN<sub>2</sub> and GeN<sub>2</sub>. *Computational Materials Science*, 95, 706–711. <https://doi.org/10.1016/j.commatsci.2014.07.003>
- Mazin, I. I., Papaconstantopoulos, D. A., & Mehl, M. J. (2002). Superconductivity in compressed iron: Role of spin fluctuations. *Physical Review B*, 65(10), 100511. <https://doi.org/10.1103/PhysRevB.65.100511>
- Moakafi, M., Khenata, R., Bouhemadou, A., Semari, F., Reshak, A. H., & Rabah, M. (2009). Elastic, electronic and optical properties of cubic antiperovskites SbNCa<sub>3</sub> and BiNCa<sub>3</sub>. *Computational Materials Science*, 46(4), 1051–1057. <https://doi.org/10.1016/j.commatsci.2009.05.011>
- Mollah, S. (2004). The physics of the non-oxide perovskite superconductor MgCNi<sub>3</sub>. *Journal of Physics Condensed Matter*, 16(43), R1237–R1276. <https://doi.org/10.1088/0953-8984/16/43/R01>
- Murnaghan, F. D. (1944). The Compressibility of Media under Extreme Pressures. *Proceedings of the National Academy of Sciences*, 30(9), 244–247. <https://doi.org/10.1073/pnas.30.9.244>

- Nyawere, P. W. O., Makau, N. W., & Amolo, G. O. (2014). First-principles calculations of the elastic constants of the cubic, orthorhombic and hexagonal phases of BaF<sub>2</sub>. *Physica B: Condensed Matter*, 434, 122–128. <https://doi.org/10.1016/j.physb.2013.10.051>
- Nye, J. F., & Lindsay, R. B. (1957). *Physical Properties of Crystals: Their Representation by Tensors and Matrices*. *Physics Today*, 10(12), 26. <https://doi.org/10.1063/1.3060200>
- Okoye, C. M. I. (2006). First-principles optical calculations of AsNMg<sub>3</sub> and SbNMg<sub>3</sub>. *Materials Science and Engineering: B*, 130(1–3), 101–107. <https://doi.org/10.1016/j.mseb.2006.02.066>
- Ortenzi, L., Biermann, S., Andersen, O. K., Mazin, I. I., & Boeri, L. (2011). Competition between electron-phonon coupling and spin fluctuations in superconducting hole-doped CuBiSO. *Physical Review B*, 83(10), 100505. <https://doi.org/10.1103/PhysRevB.83.100505>
- Ovsyannikov, S. V., & Shchennikov, V. V. (2010). High-Pressure Routes in the Thermoelectricity or How One Can Improve a Performance of Thermoelectrics. *Chemistry of Materials*, 22(3), 635–647. <https://doi.org/10.1021/cm902000x>
- Papaconstantopoulos, D. A., & Pickett, W. E. (1992). Ternary nitrides BiNCa<sub>3</sub> and PbNCa<sub>3</sub>: Unusual ionic bonding in the antiperovskite structure. *Physical Review B*, 45(8), 4008. <https://doi.org/10.1103/PhysRevB.45.4008>
- Perdew, J. P., Burke, K., & Ernzerhof, M. (1998). Perdew, Burke, and Ernzerhof Reply: *Physical Review Letters*, 80(4), 891. <https://doi.org/10.1103/PhysRevLett.80.891>
- Perdew, J. P., & Wang, Y. (1992). Accurate and simple analytic representation of the electron-gas correlation energy. *Physical Review B*, 45(23), 13244–13249. <https://doi.org/10.1103/PhysRevB.45.13244>
- Pickett, W. E. (1989). Pseudopotential methods in condensed matter applications. *Computer Physics Reports*, 9(3), 115–197. [https://doi.org/10.1016/0167-7977\(89\)90002-6](https://doi.org/10.1016/0167-7977(89)90002-6)
- Prokopenko, O. V., Bozhko, D. A., Tyberkevych, V. S., Chumak, A. V., Vasyuchka, V. I., Serga, A. A., Dzyapko, O., Verba, R. V., Talalaevskij, A. V., Slobodianiuk, D. V., Kobljanskyj, Y. V., Moiseienko, V. A., Sholom, S. V., & Malyshev, V. Y. (2019). Recent Trends in Microwave Magnetism and Superconductivity. *Ukrainian Journal of Physics*, 64(10), 888. <https://doi.org/10.15407/ujpe64.10.888>
- Pugh, S. F. (1954). XCII. Relations between the elastic moduli and the plastic properties of polycrystalline pure metals. *The London, Edinburgh, and Dublin Philosophical Magazine and Journal of Science*, 45(367), 823–843. <https://doi.org/10.1080/14786440808520496>
- Rosner, H., Weht, R., Johannes, M., Pickett, W. E., & Tosatti, E. (2001). Superconductivity near ferromagnetism in MgCNi<sub>3</sub>. <https://doi.org/10.1103/PhysRevLett.88.027001>

- Savrasov, S. Y. (1996). Linear-response theory and lattice dynamics: A muffin-tin-orbital approach. *Physical Review B*, 54(23), 16470–16486. <https://doi.org/10.1103/PhysRevB.54.16470>
- Schaak, R. E., Avdeev, M., Lee, W.-L., Lawes, G., Zandbergen, H. W., Jorgensen, J. D., Ong, N. P., Ramirez, A. P., & Cava, R. J. (2004). Formation of transition metal boride and carbide perovskites related to superconducting MgCNi<sub>3</sub>. *Journal of Solid State Chemistry*, 177(4–5), 1244–1251. <https://doi.org/10.1016/j.jssc.2003.10.032>
- Shao, D., Lu, W., Tong, P., Lin, S., Lin, J., & Sun, Y. (2014). Prediction of Superconductivity in 3 *d* Transition-Metal Based Antiperovskites via Magnetic Phase Diagram. *Journal of the Physical Society of Japan*, 83(5), 54704. <https://doi.org/10.7566/JPSJ.83.054704>
- Shim, J. H., Kwon, S. K., & Min, B. I. (2001). Electronic structures of antiperovskite superconductors MgXNi<sub>3</sub> (X= B, C, and N). *Physical Review B*, 64(18), 180510. <https://doi.org/10.1103/PhysRevB.64.180510>
- Sieberer, M., Mohn, P., & Redinger, J. (2007). Role of carbon in AlCNi<sub>3</sub> and GaCNi<sub>3</sub>: A density functional theory study. *Physical Review B*, 75(2), 024431. <https://doi.org/10.1103/PhysRevB.75.024431>
- Singh, D. J., & Mazin, I. I. (2001). Superconductivity and electronic structure of perovskite MgCNi<sub>3</sub>. *Physical Review B*, 64(14), 140507. <https://doi.org/10.1103/PhysRevB.64.140507>
- Sun, Y., Wang, C., Chu, L., Wen, Y., Nie, M., & Liu, F. (2010). Low temperature coefficient of resistivity induced by magnetic transition and lattice contraction in Mn<sub>3</sub>NiN compound. *Scripta Materialia*, 62(9), 686–689. <https://doi.org/10.1016/j.scriptamat.2010.01.027>
- Takenaka, K., & Takagi, H. (2005). Giant negative thermal expansion in Ge-doped antiperovskite manganese nitrides. *Applied Physics Letters*, 87(26). <https://doi.org/10.1063/1.2147726>
- Togo, A., & Tanaka, I. (2015). First principles phonon calculations in materials science. *Scripta Materialia*, 108, 1–5. <https://doi.org/10.1016/j.scriptamat.2015.07.021>
- Tong, P., & Sun, Y. P. (2012). Research Progress on Ni-Based Antiperovskite Compounds. *Advances in Condensed Matter Physics*, 2012, 1–9. <https://doi.org/10.1155/2012/903239>
- Tran, F., Laskowski, R., Blaha, P., & Schwarz, K. (2007). Performance on molecules, surfaces, and solids of the Wu-Cohen GGA exchange-correlation energy functional. *Physical Review B*, 75(11), 115131. <https://doi.org/10.1103/PhysRevB.75.115131>
- Turquette, A. R. (1958). Max Black. Abstract and abstraction. Encyclopaedia Britannica, Encyclopaedia Britannica, Inc., Chicago-London-Toronto 1956, Vol. 1, pp. 67–68; also Max Black. *Abstract and abstraction*. **Encyclopaedia Britannica**, Encyclopaedia Britannica, In. *Journal of Symbolic Logic*, 23(1), 22–29. <https://doi.org/10.2307/2964454>

- Vaghela, M. V, Raval, D., Babariya, B., & Gajjar, P. N. (2022). Computational study of structural, electronic and optical properties of HgIn amalgam. *Physica B: Condensed Matter*, 639, 413882. <https://doi.org/10.1016/j.physb.2022.413882>
- Vosko, S. H., Wilk, L., & Nusair, M. (1980). Accurate spin-dependent electron liquid correlation energies for local spin density calculations: a critical analysis. *Canadian Journal of Physics*, 58(8), 1200–1211. <https://doi.org/10.1139/p80-159>
- Wälte, A., Fuchs, G., Müller, K. H., Handstein, A., Nenkov, K., Narozhnyi, V. N., ...&Rosner, H. (2004). Evidence for strong electron-phonon coupling in MgCNi<sub>3</sub>. *Physical Review B*, 70(17), 174503. <https://doi.org/10.1103/PhysRevB.70.174503>
- Wang, Y., & Perdew, J. P. (1991). Spin scaling of the electron-gas correlation energy in the high-density limit. *Physical Review B*, 43(11), 8911–8916. <https://doi.org/10.1103/PhysRevB.43.8911>
- Wiendlocha, B., Tobola, J., Kaprzyk, S., & Fruchart, D. (2007). Electronic structure, superconductivity and magnetism study of Cr<sub>3</sub>GaN and Cr<sub>3</sub>RhN. *Journal of Alloys and Compounds*, 442(1–2), 289–291. <https://doi.org/10.1016/j.jallcom.2006.08.365>
- Wright, W. W. (1993). Materials science and engineering. An introduction 2nd Edition W. D. Callister, Jr John Wiley & Sons, New York, 1991. pp. xxi + 791, price E53.00. ISBN 0-471-50488-2. *Polymer International*, 30(2), 282–283. <https://doi.org/10.1002/pi.4990300228>
- Wright, W. W., Wang, Y., Perdew, J. P., Vosko, S. H., Wilk, L., Nusair, M., Vaghela, M. V, Raval, D., Babariya, B., Gajjar, P. N., Turquette, A. R., Tran, F., Laskowski, R., Blaha, P., Schwarz, K., Tütüncü, H. M., Srivastava, G. P., Togo, A., Tanaka, I., ... Whitfield, J. (2014). Theory for superconductivity in Pd-H and Pd-D systems. *Physica B: Condensed Matter*, 260(5), 122–128. <https://doi.org/10.1007/BF01397961>
- Wu, M. K., Ashburn, J. R., Torng, C. J., Hor, P. H., Meng, R. L., Gao, L., Huang, Z. J., Wang, Y. Q., & Chu, C. W. (1987). Superconductivity at 93 K in a new mixed-phase Y-Ba-Cu-O compound system at ambient pressure. *Physical Review Letters*, 58(9), 908–910. <https://doi.org/10.1103/PhysRevLett.58.908>
- Yang, J., & Whitfield, J. (2023). Machine-learning Kohn-Sham potential from dynamics in time-dependent Kohn-Sham systems. *Machine Learning: Science and Technology*. <https://doi.org/10.1088/2632-2153/ace8f0>



## APPENDICES

### Appendix I: Input File for Pwscf Code AlCCr3 Structure

&control

```
calculation = 'scf',  
prefix = 'x',  
restart_mode = 'from_scratch',  
outdir = './'  
pseudo_dir = './'  
verbosity = 'high'  
wf_collect = .true.  
etot_conv_thr=1.0D-44  
forc_conv_thr= 1.0D-3  
/
```

&system

```
ibrav = 4,  
celldm(1) = 5.2,  
celldm(3) = 4.47,  
nat = 8,  
ntyp = 3,  
ecutwfc = 32  
ecutrho = 650  
input_dft = 'BLYP',  
occupations= 'smearing'  
smearing = 'gaussian',  
degauss = 0.01  
/
```

&electrons

```
electron_maxstep = 100  
mixing_mode='plain'  
mixing_beta = 0.7  
diagonalization='david'  
conv_thr = 1.0d-10  
/
```

ATOMIC\_SPECIES

Cr 51.9961 Cr.pbe-spn-kjpaw\_psl.1.0.0.UPF

Al 26.98 Al.pbe-n-kjpaw\_psl.1.0.0.UPF

C 12.0107 C.pbe-n-kjpaw\_psl.1.0.0.UPF

ATOMIC\_POSITIONS (crystal)

Cr 0.666667000 0.333334000 0.913761657

Cr 0.333333000 0.666666000 0.413761657

Cr 0.333333000 0.666666000 0.086238343

Cr 0.666667000 0.333334000 0.586238343

Al 0.666667000 0.333334000 0.250000000

Al 0.333333000 0.666666000 0.750000000

C -0.000000000 -0.000000000 -0.000000000

C -0.000000000 0.000000000 0.500000000

K\_POINTS (automatic)

18 18 4 1 1 1

## Appendix II: Input File for Pwscf Code GaCCr3 Structure

```
&control
calculation = 'scf',
prefix = 'x',
restart_mode = 'from_scratch',
outdir = './'
pseudo_dir = './'
verbosity = 'high'
wf_collect = .true.
etot_conv_thr=1.0D-5
forc_conv_thr= 1.0D-4
/
&system
ibrav = 4,
celldm(1) = 5.8,
celldm(3) = 4.4,
nat = 8,
ntyp = 3,
ecutwfc = 38
ecutrho = 720
input_dft = 'BLYP',
occupations='smearing'
smearing = 'gaussian',
degauss = 0.01
/
&electrons
electron_maxstep = 100
mixing_mode='plain'
mixing_beta = 0.3
diagonalization='david'
conv_thr = 1.0d-8
/
ATOMIC_SPECIES
```

Cr 51.9961 Cr.pbe-spn-kjpaw\_psl.1.0.0.UPF

Ga 69.72 Ga.pbe-dn-kjpaw\_psl.1.0.0.UPF

C 12.0107 C.pbe-n-kjpaw\_psl.1.0.0.UPF

ATOMIC\_POSITIONS (crystal)

Cr 0.666667000 0.333334000 0.913761657

Cr 0.333333000 0.666666000 0.413761657

Cr 0.333333000 0.666666000 0.086238343

Cr 0.666667000 0.333334000 0.586238343

Ga 0.666667000 0.333334000 0.250000000

Ga 0.333333000 0.666666000 0.750000000

C -0.000000000 -0.000000000 -0.000000000

C -0.000000000 0.000000000 0.500000000

K\_POINTS (automatic)

22 22 4 1 1 1

### Appendix III: Input File for Pwscf Code ZnCCr3 Structure

```
&control
calculation = 'scf',
prefix = 'x',
restart_mode = 'from_scratch',
outdir = './'
pseudo_dir = './'
verbosity = 'high'
wf_collect = .true.
etot_conv_thr=1.0D-4
forc_conv_thr= 1.0D-3
/
&system
ibrav = 4,
celldm(1) = 5.7,
celldm(3) = 4.6,
nat = 8,
ntyp = 3,
ecutwfc = 35
ecutrho = 720
input_dft = 'BLYP',
occupations='smearing'
smearing = 'gaussian',
degauss = 0.01
/
&electrons
electron_maxstep = 100
mixing_mode='plain'
mixing_beta = 0.4
diagonalization='david'
conv_thr = 1.0d-12
/
ATOMIC_SPECIES
```

Cr 51.9961 Cr.pbe-spn-kjpaw\_psl.1.0.0.UPF

Zn 65.39 Zn.pbe-dnl-kjpaw\_psl.1.0.0.UPF

C 12.0107 C.pbe-n-kjpaw\_psl.1.0.0.UPF

ATOMIC\_POSITIONS (crystal)

Cr 0.666667000 0.333334000 0.913761657

Cr 0.333333000 0.666666000 0.413761657

Cr 0.333333000 0.666666000 0.086238343

Cr 0.666667000 0.333334000 0.586238343

Zn 0.666667000 0.333334000 0.250000000

Zn 0.333333000 0.666666000 0.750000000

C -0.000000000 -0.000000000 -0.000000000

C -0.000000000 0.000000000 0.500000000

K\_POINTS (automatic)

18 18 4 1 1 1

#### Appendix IV: Output File for AlCCr3 Structure

Elastic constant 1 1

strain stress (kbar)

-0.0075000000 -1168.5141954263

-0.0025000000 -1181.8610573920

0.0025000000 -1193.3371441526

0.0075000000 -1205.2374727655

Polynomial coefficients

a1= -0.807375053856E-02

a2= -0.165386457440E-01

a3= 0.983333551925E-01

-----

Elastic constant 2 1

strain stress (kbar)

-0.0075000000 -1189.8557034752

-0.0025000000 -1189.4008323065

0.0025000000 -1187.485525722

0.0075000000 -1185.8187780236

Polynomial coefficients

a1= -0.807938887165E-02

a2= 0.190694414718E-02

a3= 0.823835311502E-01

-----

Elastic constant 3 1

strain stress (kbar)

-0.0075000000 -1221.7079101057

-0.0025000000 -1220.8019618687

0.0025000000 -1219.5485199763

0.0075000000 -1218.5299124508

Polynomial coefficients

a1= -0.829463195720E-02

a2= 0.146663008000E-02

a3= 0.765842405645E-02

-----

Elastic constant 3 3

strain stress (kbar)

-0.0075000000 -1205.8022535485

-0.0025000000 -1215.9761845493

0.0025000000 -1225.0276153553

0.0075000000 -1234.7773681235

Polynomial coefficients

a1= -0.829698489447E-02

a2= -0.130487392390E-01

a3= 0.288350550108E-01

-----

Elastic constant 5 5

strain stress (kbar)

-0.0075000000 17.3536951343

-0.0025000000 6.2252691413

0.0025000000 -6.2252764667

0.0075000000 -17.3536238260

Polynomial coefficients

a1= -0.583073511685E-10



$$a_2 = -0.158488779691E-01$$

$$a_3 = 0.534540739742E-05$$

-----

Elastic constants  $C_{ij}$  (kbar)

ij=	1	2	3	4	5	6
1	2432.91838	-280.52112	-215.74870	0.00000	0.00000	0.00000
2	-280.52112	2432.91838	-215.74870	0.00000	0.00000	0.00000
3	-215.74870	-215.74870	1919.53549	0.00000	0.00000	0.00000
4	0.00000	0.00000	0.00000	1165.72502	0.00000	0.00000
5	0.00000	0.00000	0.00000	0.00000	1165.72502	0.00000
6	0.00000	0.00000	0.00000	0.00000	0.00000	1356.71975

$$1 \text{ bar} = 10^5 \text{ Pa}; 10 \text{ kbar} = 1 \text{ GPa}; 1 \text{ atm} = 1.01325 \text{ bar}; 1 \text{ Pa} = 1 \text{ N/m}^2$$

$$1 \text{ Pa} = 10 \text{ dyn/cm}^2; 1 \text{ Mbar} = 10^{11} \text{ Pa}$$

$$1 \text{ torr} = 1 \text{ mm Hg} = 1/760 \text{ bar} = 7.5006 \times 10^{-3} \text{ Pa}$$

-----

Elastic compliances  $S_{ij}$  (1/Mbar)

ij=	1	2	3	4	5	6
1	0.42192	0.05339	0.05342	0.00000	0.00000	0.00000
2	0.05339	0.42192	0.05342	0.00000	0.00000	0.00000
3	0.05342	0.05342	0.53297	0.00000	0.00000	0.00000
4	0.00000	0.00000	0.00000	0.85784	0.00000	0.00000
5	0.00000	0.00000	0.00000	0.00000	0.85784	0.00000
6	0.00000	0.00000	0.00000	0.00000	0.00000	0.73707

$$1/\text{Mbar} = 1/10^{11} \text{ Pa}; 1 \text{ Pa} = 1 \text{ N/m}^2$$

-----

Voigt approximation:

$$\text{Bulk modulus } B = 595.70391 \text{ kbar}$$

$$\text{Young modulus } E = 2193.51316 \text{ kbar}$$

$$\text{Shear modulus } G = 1237.46001 \text{ kbar}$$

Poisson Ratio  $n = 0.11370$

Reuss approximation:

Bulk modulus  $B = 589.17933$  kbar

Young modulus  $E = 2172.76575$  kbar

Shear modulus  $G = 1227.03906$  kbar

Poisson Ratio  $n = -0.11463$

Voigt-Reuss-Hill average of the two approximations:

Bulk modulus  $B = 592.44162$  kbar

Young modulus  $E = 2183.13945$  kbar

Shear modulus  $G = 1232.24953$  kbar

Poisson Ratio  $n = 0.11417$

Voigt-Reuss-Hill average; sound velocities:

Compressional  $V_P = 6790.410$  m/s

Bulk  $V_B = 3495.724$  m/s

Shear  $V_G = 5041.546$  m/s

The approximate Debye temperature is  $719.587$  K

-----  
Average Debye sound velocity =  $5416.127$  m/s

Debye temperature =  $718.557$  K

++++  
++++

Computing the thermodynamic properties from elastic constants

Writing on file therm\_files/output\_therm.dat\_debye.g1

++++  
++++

THERMO\_PW : 2h39m CPU 2h53m WALL

This run was terminated on: 1:16:27 31Dec2022

## Appendix V: Output File for GaCCr3 Structure

Elastic constant 1 1

strain stress (kbar)

-0.0075000000	-318.0726532137
-0.0025000000	-328.1437649953
0.0025000000	-337.5442132438
0.0075000000	-346.5876640142

Polynomial coefficients

a1= -0.226306444842E-02

a2= -0.129085273492E-01

a3= 0.698589873832E-01

-----

Elastic constant 2 1

strain stress (kbar)

-0.0075000000	-330.8202240278
-0.0025000000	-332.0996842507
0.0025000000	-333.5330010646
0.0075000000	-334.9606834341

Polynomial coefficients

a1= -0.226237691828E-02

a2= -0.188364636757E-02

a3= -0.100759384210E-01

-----

Elastic constant 3 1

strain stress (kbar)

-0.0075000000	-377.7118751080
-0.0025000000	-379.3916237811
0.0025000000	-380.6994144552
0.0075000000	-382.0826077603

Polynomial coefficients

a1= -0.258362335927E-02

a2= -0.196050213598E-02

a3= 0.201594275561E-01

-----

Elastic constant 3 3

strain stress (kbar)

-0.0075000000 -366.0953021389

-0.0025000000 -375.3890607145

0.0025000000 -384.1622994356

0.0075000000 -392.8429676847

Polynomial coefficients

a1= -0.258192351551E-02

a2= -0.121024034085E-01

a3= 0.416770403042E-01

-----

Elastic constant 5 5

strain stress (kbar)

-0.0075000000 9.6343451669

-0.0025000000 3.2149049905

0.0025000000 -3.2149748440

0.0075000000 -9.6343633687

Polynomial coefficients

a1= -0.259372073048E-09

a2= -0.873335125974E-02

a3= 0.351120882762E-05

-----

Elastic constants  $C_{ij}$  (kbar)

$ij=$	1	2	3	4	5	6
1	1898.90961	277.09390	288.39977	0.00000	0.00000	0.00000
2	277.09390	1898.90961	288.39977	0.00000	0.00000	0.00000
3	288.39977	288.39977	1780.32471	0.00000	0.00000	0.00000
4	0.00000	0.00000	0.00000	642.36005	0.00000	0.00000
5	0.00000	0.00000	0.00000	0.00000	642.36005	0.00000
6	0.00000	0.00000	0.00000	0.00000	0.00000	810.90786

1 bar =  $10^5$  Pa; 10 kbar = 1 GPa; 1 atm = 1.01325 bar; 1 Pa = 1 N/m<sup>2</sup>

1 Pa = 10 dyn/cm<sup>2</sup>; 1 Mbar =  $10^{11}$  Pa

1 torr = 1 mm Hg = 1/760 bar =  $7.5006 \times 10^{-3}$  Pa

-----

Elastic compliances  $S_{ij}$  (1/Mbar)

$ij=$	1	2	3	4	5	6
1	0.54838	-0.06821	-0.07779	0.00000	0.00000	0.00000
2	-0.06821	0.54838	-0.07779	0.00000	0.00000	0.00000
3	-0.07779	-0.07779	0.58690	0.00000	0.00000	0.00000
4	0.00000	0.00000	0.00000	1.55676	0.00000	0.00000
5	0.00000	0.00000	0.00000	0.00000	1.55676	0.00000
6	0.00000	0.00000	0.00000	0.00000	0.00000	1.23319

1/Mbar =  $1/10^{11}$  Pa; 1 Pa = 1 N/m<sup>2</sup>

-----

Voigt approximation:

Bulk modulus  $B = 809.54787$  kbar

Young modulus  $E = 1691.08411$  kbar

Shear modulus  $G = 734.07563$  kbar

Poisson Ratio  $n = 0.15185$

Reuss approximation:

Bulk modulus  $B = 808.98983$  kbar

Young modulus E = 1675.95025 kbar  
Shear modulus G = 725.69321 kbar  
Poisson Ratio n = 0.15472

Voigt-Reuss-Hill average of the two approximations:

Bulk modulus B = 809.26885 kbar  
Young modulus E = 1683.51718 kbar  
Shear modulus G = 729.88442 kbar  
Poisson Ratio n = 0.15328

Voigt-Reuss-Hill average; sound velocities:

Compressional V\_P = 5340.797 m/s  
Bulk V\_B = 3598.687 m/s  
Shear V\_G = 3417.627 m/s

The approximate Debye temperature is 483.799 K

-----  
Average Debye sound velocity = 3750.006 m/s

Debye temperature = 483.170 K

++++  
++++

Computing the thermodynamic properties from elastic constants

Writing on file therm\_files/output\_therm.dat\_debye.g1

++++  
++++

THERMO\_PW : 12h58m CPU 13h50m WALL

This run was terminated on: 12: 2:31 31Dec2022

## Appendix VI: Output File for ZnCCr3 Structure

Elastic constant 1 1

strain stress (kbar)  
-0.0075000000 -650.5842944556  
-0.0025000000 -660.3687937512  
0.0025000000 -669.6720626358  
0.0075000000 -678.7243795885

Polynomial coefficients

a1= -0.452102882547E-02  
a2= -0.127423935104E-01  
a3= 0.497727523906E-01

-----  
Elastic constant 2 1

strain stress (kbar)  
-0.0075000000 -666.6818814222  
-0.0025000000 -665.5031579448  
0.0025000000 -664.3743794025  
0.0075000000 -663.4501387469

Polynomial coefficients

a1= -0.452005451433E-02  
a2= 0.147160226963E-02  
a3= -0.172993935239E-01

-----  
Elastic constant 3 1

strain stress (kbar)  
-0.0075000000 -707.8744543373  
-0.0025000000 -707.3401555012  
0.0025000000 -706.7007118764  
0.0075000000 -706.3056486987

Polynomial coefficients

a1= -0.480616887147E-02

a2= 0.726808548690E-03

a3= -0.946504927483E-02

-----  
Elastic constant 3 3

strain stress (kbar)

-0.0075000000 -698.5554848677

-0.0025000000 -704.3452954663

0.0025000000 -709.9239152904

0.0075000000 -714.2937360746

Polynomial coefficients

a1= -0.480760745754E-02

a2= -0.717764237225E-02

a3= 0.965289618233E-01

-----  
Elastic constant 5 5

strain stress (kbar)

-0.0075000000 10.9969248336

-0.0025000000 4.3265864233

0.0025000000 -4.3265858639

0.0075000000 -10.9969579249

Polynomial coefficients

a1= 0.161983104579E-10

a2= -0.101471456655E-01

a3= -0.228752767355E-05

-----  
Elastic constants C\_ij (kbar)



ij=	1	2	3	4	5	6
1	1874.47049	-216.48013	-106.91721	0.00000	0.00000	0.00000
2	-216.48013	1874.47049	-106.91721	0.00000	0.00000	0.00000
3	-106.91721	-106.91721	1055.86747	0.00000	0.00000	0.00000
4	0.00000	0.00000	0.00000	746.34821	0.00000	0.00000
5	0.00000	0.00000	0.00000	0.00000	746.34821	0.00000
6	0.00000	0.00000	0.00000	0.00000	0.00000	1045.47531

1 bar =  $10^5$  Pa; 10 kbar = 1 GPa; 1 atm = 1.01325 bar; 1 Pa = 1 N/m<sup>2</sup>

1 Pa = 10 dyn/cm<sup>2</sup>; 1 Mbar =  $10^{11}$  Pa

1 torr = 1 mm Hg = 1/760 bar =  $7.5006 \times 10^{-3}$  Pa

-----  
Elastic compliances  $S_{ij}$  (1/Mbar)

ij=	1	2	3	4	5	6
1	0.54469	0.06643	0.06188	0.00000	0.00000	0.00000
2	0.06643	0.54469	0.06188	0.00000	0.00000	0.00000
3	0.06188	0.06188	0.95962	0.00000	0.00000	0.00000
4	0.00000	0.00000	0.00000	1.33986	0.00000	0.00000
5	0.00000	0.00000	0.00000	0.00000	1.33986	0.00000
6	0.00000	0.00000	0.00000	0.00000	0.00000	0.95650

1/Mbar =  $1/10^{11}$  Pa; 1 Pa = 1 N/m<sup>2</sup>

-----  
Voigt approximation:

Bulk modulus  $B = 438.24215$  kbar

Young modulus  $E = 1556.04682$  kbar

Shear modulus  $G = 856.64254$  kbar

Poisson Ratio  $\nu = 0.09178$

Reuss approximation:

Bulk modulus  $B = 411.62575$  kbar

Young modulus E = 1475.85577 kbar  
Shear modulus G = 817.71373 kbar  
Poisson Ratio n = 0.09757

Voigt-Reuss-Hill average of the two approximations:

Bulk modulus B = 424.93395 kbar  
Young modulus E = 1515.95130 kbar  
Shear modulus G = 837.17814 kbar  
Poisson Ratio n = 0.09461

Voigt-Reuss-Hill average; sound velocities:

Compressional V\_P = 5001.938 m/s  
Bulk V\_B = 2626.477 m/s  
Shear V\_G = 3686.564 m/s

The approximate Debye temperature is 513.282 K

-----  
Average Debye sound velocity = 3940.871 m/s

Debye temperature = 509.329 K

++++  
++++

Computing the thermodynamic properties from elastic constants  
Writing on file therm\_files/output\_therm.dat\_debye.g1

++++  
++++

THERMO\_PW : 8h50m CPU 9h25m WALL

This run was terminated on: 16:32:50 10 Jan2023

Appendix VII: Introduction letter from the institution



KABARAK UNIVERSITY  
INSTITUTE OF POSTGRADUATE STUDIES  
OFFICE OF THE DIRECTOR

Private Bag - 20157  
KABARAK, KENYA  
<http://kabarak.ac.ke/institute-postgraduate-studies/>

Tel: 0773265999  
E-mail: [directorpostgraduate@kabarak.ac.ke](mailto:directorpostgraduate@kabarak.ac.ke)

22<sup>nd</sup> September 2022

The Chairman  
Research and Ethics Committee (KUREC)  
Kabarak University

Dear Sir,

**RE: MAINA N. DAVID - GMP/M/0345/01/20**

The above named is a candidate at Kabarak University pursuing Masters in Physics. He is carrying out a research entitled "*Ab initio Calculations of Electronic and Superconductivity properties of Cubic Antiperovskite Materials AXCR<sub>3</sub> (X = C OR N, a = Zn, Ga, Al)*".

The student has defended his proposal and has been authorised to proceed with field research.

Kindly provide the KUREC clearance to enable the student obtain NACOSTI research permit.

Thank you

**DR. WILSON O. SHITANDI**  
**DIRECTOR, POSTGRADUATE STUDIES**



**Kabarak University Moral Code**

*As members of Kabarak University family, we purpose at all times and in all places, to set apart in one's heart,  
Jesus as Lord. (1 Peter 3:15)*



Kabarak University is ISO 9001:2015 Certified

## Appendix VIII: KUREC Clearance Letter



### KABARAK UNIVERSITY RESEARCH ETHICS COMMITTEE

Private Bag - 20157  
KABARAK, KENYA  
Email: [kurec@kabarak.ac.ke](mailto:kurec@kabarak.ac.ke)

Tel: 254-51-343234/5  
Fax: 254-051-343529  
[www.kabarak.ac.ke](http://www.kabarak.ac.ke)

OUR REF: KABU01/KUREC/001/04/02/23

Date: 10<sup>th</sup> February, 2023

Maina Njuguna David,  
Reg. No: GMP/M/0345/01/20  
Kabarak University,

Dear David,

**RE: Ab INITIO CALCULATIONS OF ELECTRONIC AND SUPERCONDUCTIVITY PROPERTIES OF CUBIC ANTIPEROVSKITE MATERIALS  $AXCr_3$  (X=C or N, A=Zn, Ga or Al)**

This is to inform you that **KUREC** has reviewed and approved your above research proposal. Your application approval number is **KUREC-040223**. The approval period is **10/02/2023 – 10/02/2024**.

This approval is subject to compliance with the following requirements:

- i. All researchers shall obtain an introduction letter to NACOSTI from the relevant head of institutions (Institute of postgraduate, School dean or Directorate of research)
- ii. The researcher shall further obtain a RESEARCH PERMIT from NACOSTI before commencement of data collection & submit a copy of the permit to **KUREC**.
- iii. Only approved documents including (informed consents, study instruments, MTA Material Transfer Agreement) will be used
- iv. All changes including (amendments, deviations, and violations) are submitted for review and approval by **KUREC**.
- v. Death and life-threatening problems and serious adverse events or unexpected adverse events whether related or unrelated to the study must be reported to **KUREC** within 72 hours of notification;
- vi. Any changes, anticipated or otherwise that may increase the risk(s) or affected safety or welfare of study participants and others or affect the integrity of the research must be reported to **KUREC** within 72 hours;
- vii. Clearance for export of biological specimens must be obtained from relevant institutions and submit a copy of the permit to **KUREC**;
- viii. Submission of a request for renewal of approval at least 60 days prior to expiry of the approval period. Attach a comprehensive progress report to support the renewal and;
- ix. Submission of an executive summary report within 90 days upon completion of the study to **KUREC**

Sincerely,

  
**Prof. Jackson Kitetu PhD.**  
KUREC-Chairman

Cc Vice Chancellor  
DVC-Academic & Research  
Registrar-Academic & Research  
Director-Research Innovation & Outreach  
Institute of Post Graduate Studies



*As members of Kabarak University family, we purpose at all times and in all places, to set apart in one's heart, Jesus as Lord.*  
(1 Peter 3:15)



Kabarak University is ISO 9001:2015 Certified

## Appendix IX: NACOSTI Research Permit

 REPUBLIC OF KENYA	 NATIONAL COMMISSION FOR SCIENCE, TECHNOLOGY & INNOVATION
Ref No: <b>229551</b>	Date of Issue: <b>31/March/2023</b>
<b>RESEARCH LICENSE</b>	
	
<p>This is to Certify that Mr. David Maina Njuguna of Kabarak University, has been licensed to conduct research as per the provision of the Science, Technology and Innovation Act, 2013 (Rev.2014) in Nakuru on the topic: <b>Ab initio calculations of electronic and superconductivity properties of cubic Antiperovskite materials AXCr3 (X=C or N, A=Zn, Ga or Al), for the period ending : 31/March/2024.</b></p>	
License No: <b>NACOSTI/P/23/24000</b>	
229551 Applicant Identification Number	 Director General NATIONAL COMMISSION FOR SCIENCE, TECHNOLOGY & INNOVATION
Verification QR Code	
	
<p>NOTE: This is a computer generated License. To verify the authenticity of this document, Scan the QR Code using QR scanner application.</p>	
See overleaf for conditions	



**Appendix X: Evidence of Conference Participation**



Scanned by CamScanner

## Appendix XI: List of Publications

Kabarak Journal of Research & Innovation  
www.kabarak.ac.ke

RESEARCH ARTICLE

### First-principles Calculation of Elastic and Electronic Structure Properties of Hexagonal Antiperovskite-type Carbides $\text{XCCr}_3$ (X=Al, Ga or Zn) Materials

David MAINA NJUGUNA<sup>1\*</sup>, Phillip OTIENO NYAWERE<sup>2</sup>, and Elicah WABULULU<sup>3</sup>

<sup>1</sup>Department of Physical and Biological Sciences, Kabarak University, P.O. Box Private Bag – 20157 Kabarak, Nakuru, Kenya

<sup>1</sup>[mainadavid964@gmail.com](mailto:mainadavid964@gmail.com)

<sup>2</sup>Department of Physical and Biological Sciences, Kabarak University, P.O. Box Private Bag – 20157 Kabarak, Nakuru, Kenya

<sup>2</sup>[nyawere@gmail.com](mailto:nyawere@gmail.com)

<sup>3</sup>Department of Natural Sciences, Catholic University of Eastern Africa, P.O. Box 62547, Nairobi, Kenya

<sup>3</sup>[ewabululu@cuea.edu](mailto:ewabululu@cuea.edu)

Submitted 18<sup>th</sup> January 2023, Accepted 20<sup>th</sup> February 2023 and Published 29<sup>th</sup> March 2023

#### ABSTRACT

Hexagonal chromium based Antiperovskite materials have been attracting a lot of research interest lately as a result of their superconducting properties. In this study the elastic and electronic structure properties of  $\text{XCCr}_3$  (X= Al, Ga or Zn) were investigated using first principles density functional theory within the generalized gradient approximations using Quantum Espresso code. Shear Modulus (G), Young's Modulus (E), Bulk modulus (B), Poisson ratios ( $\nu$ ) and Zener anisotropy factor (A) values are calculated and evaluated in calculations of elastic properties. Mechanical stability and stiffness of these materials are determined and  $\text{XCCr}_3$  (X= Al, Ga or Zn) compounds are found to be mechanically stable at zero pressure. The Fermi level locates at the vicinity of density of states (DOS) peak, which leads large DOS at the Fermi level  $N(E_F)$  with values of 4.89, 5.72 and 4.32 states/eV for  $\text{AlCCr}_3$ ,  $\text{GaCCr}_3$  and  $\text{ZnCCr}_3$  respectively. The band structures are similar to that of superconducting Antiperovskite  $\text{MgCNi}_3$ .

**Key Words:** Antiperovskite, Elastic, Mechanical stability